CERN/DRDC/93-46
RD-6/Status Report
November 9, 1993

INTEGRATED TRANSITION RADIATION AND TRACKING DETECTOR FOR LHC

(Transition Radiation Tracker)

V. Commishau, K. Hangarter, V. Kashevarov, M. Tonutti, R. Schulte
Aachen TH, III Phys. Inst., Germany

R.K. Bock, E. David, N.D. Dixon, C.W. Fabjan, Ph. Farthouat, D. Froidevaux, W. Fuchs, W. Funk, C. Hauviller, P. Lichard, P. Nevski, G. Poulard, M.J. Price, S. Schuh.
CERN, Geneva, Switzerland

C. Raine, D. Saxon, I.O. Skillicorn, M. Stavrianakou, A. Wilson
Glasgow University, U.K.

V. Bychkov, E. Novikov, V. Peshekhonov, Yu. Zlobin
JINR (Dubna), Russia

K. Cetnar, J. Chwastowski, S. Jagelski, P. Malecki, Z. Natkaniec
Institute of Nuclear Physics, Krakow, Poland

M.B. Ishmuhametov, V.G. Ivochkin, V.V. Gromov, A.V. Nadtochi, E.M. Spiridenkov, V.L. Stepanov, V.A. Schegelsky
Nuclear Physics Institute, St. Petersbourg, Russia

T. Akesson, H. Carling, H. Danielson, B. Lundberg, U. Mjörnmark, M. Thulesius
University of Lund, Sweden

V. Bashkirov, V. Bondarenko, B. Dolgoshein, S. Furletov, D. Gavritenkov, V. Grigoriev, V. Kolodyazhny, O. Kondratiev, A. Konstantinov, S. Pavlenko, A. Romaniouk, S. Semenov, S. Smirnov, V. Sosnovtsev
Moscow Physical Engineering Institute, Moscow, Russia

S. Konovalov, M. Kopitin, S. Muraviev, A. Shmeleva, L. Vasilieva
P.N. Lebedev Institute of Physics, Moscow, Russia

H. Brettel, B. Dulny, F. Dydak, J. Fent, K. Jakobs, R. Richter, R. St. Denis
MPI, Munich, Germany

B.J. Claxton, R.W. Clifft, J.G. Dowdell, S. Jaroslawski, P. Norton, D.J. White
Rutherford Appleton Laboratory, Didcot, U.K.

G. Gillesen, M. Holder, A. Kreutz
Siegen University, Germany

1. Introduction

The RD6 collaboration is developing a straw tracker with integrated transition radiation capability for an experiment at the LHC. This continuous tracker is based on the fact that pile-up detector hits are rather uncorrelated when searching for high momentum tracks in a magnetic field, and therefore, a large number of measurement planes gives a low probability of fake tracks. There is space for a radiator between the straw planes since the straws are spread over a large radial region. This gives one to two orders of magnitude (depending on luminosity and electron transverse momentum p_T) enhancement of the electron identification at the cost of about 4% of a radiation length.

The proposal for R&D on an Integrated Tracker and Transition Radiation Detector, TRT, was submitted to the DRDC on 29th August 1990 [1]. The project was approved by the Research Board as RD6. A first status report [2] was presented at the tenth DRDC meeting and was approved with the recommendation that the demonstration of the system approach should be the main activity in 1992 and 1993.

This status report presents the work of the RD6 Collaboration following the recommendations: production of prototypes, development of electronics, performance studies using the analysis of test beam data, system simulation and radiation resistance determination.

Which prototypes should be built must be determined by the way one envisages the TRT layout in an LHC experiment. The radial extension of the TRT is 0.5-1.0 m and the axial extension is about ± 3.5 m. The orientation of the straws has to be changed at ~ 45º polar angle since the particles should traverse the detectors with an angle as large as possible. The layout therefore has radial straws in the endcap region and axial straws in the barrel region.

The RD6 collaboration has decided to build prototypes demonstrating the technical feasibility of the TRT in the endcap region. These prototypes should demonstrate:

i. the performance of the detector when measuring particles in a magnetic field with an LHC-adapted readout system;
ii. the mechanical and electrical properties, accuracy of wire/straw positions, and assembly procedure of such an instrument, using very light and robust materials.

The first point requires a prototype with a large number of layers while the second point requires one module or wheel with full azimuthal coverage. The RD6 collaboration therefore decided to build two different prototypes: an azimuthal slice of a reduced size long sector to be tested in a magnetic field and a full-scale prototype of one wheel.

The TRT work has now become a joint effort between RD6 and the ATLAS collaboration [3]. The TRT boundary conditions are imposed by the optimisation of the ATLAS inner detector in which the TRT is part of the baseline design [4].

Over the last few years, the TRT development has led to some conceptual changes in the detector approach. The most important of these changes is the use of the straw detectors as drift chambers giving a resolution of about 150 μm. This has strong implications for the TRT as an LHC tracking detector. The first two blocks (1024 straws) of the sector prototype was installed in the H8 test beam in October 1993 and the full six module prototype will be ready by spring 1994.

The wheel prototype will be ready in May 1994. We expect that these prototypes are the last within the framework of RD6 for the radial straw geometry, and that the next step will be the construction of ATLAS inner detector prototypes.

This Status Report is organised as follows: Section 2 describes systematic studies of straw properties; Section 3 presents the results of the analysis of test beam data collected in 1991-1992, including the performance of the TRT in a magnetic field with a drift-time measurement for tracking (it had not been included as a milestone in 1991), particle identification and pattern recognition results. Section 4 presents the most relevant Monte Carlo (MC) results on the TRT performance in ATLAS and Section 5 describes the status of the construction of the sector prototype and of the full-scale LHC prototype as well as future plans. Section 6 describes the TRT electronics and the Level-2 triggering. Finally Section 7 presents the milestones as well as the budget/test beam/computer requests for 1994.

2. Systematic Study of Straw Proportional Tubes [5]

2.1 Mechanical properties of the straw tubes

The proportional straw tubes for the TRT detector are prepared from a Kapton film containing a conductive layer on one side (1000 to 3000 Angs. Al + 4 μm Carbon-loaded Kapton), and a thermoplastic polyurethane layer of ~ 3 μm on the other side. The manufacturing process is performed on a precisely tooled mandrel, on which two Kapton-film tapes (4-8 mm wide) are wound on spirals at a temperature of ~ 200ºC, as shown in Fig. 1. This process may provide straws of up to 5 m length. A cut through the straw wall is shown in Fig. 2. The total resulting straw wall thickness is about 60 μm. The straw wall thus has conductive layers on both sides. The properties of such straws have been investigated and some basic characteristics are given in Table 1.

Studies have shown that to keep the straw straight it has to be stretched by a force not less than 200 g. The problem which may then arise is that the straw material may flow with time; this would reduce the original straw tension and could be a major source of concern for the long term stability of a large system. The way to solve the problem of long term straw instability (due to humidity, temperature, load etc.) has been developed at CERN for the full-scale TRT wheel engineering prototype (see Section 5.2). It consists in reinforcing the straw walls with carbon fibres which are glued on the straw. Some of the mechanical properties of such reinforced straws are given in Table 2.

2.2 Electrical properties of the straw tubes

The most important electrical characteristics of the straws are given in Table 3. More detailed information about the straw electrical properties may be found in [6,7,8]; a summary of current knowledge is presented here. As already mentioned, there are two conductive layers in the straw, placed on the inside and outside surfaces of the straw wall. Such a design does not result in any significant increase of the straw material thickness but gives additional robustness in case of cathode conductive layer damage (for example due to accidental breakdowns). It has been shown experimentally that after several breakdowns at one point in the straw, the resistance of the inner cathode layer sharply increases (up to 30 kΩ) which is fatal for a straw with one single conductive layer. On the other hand, the fast signal propagation characteristics of a straw with a double conductive layer remain unchanged in the same situation.

These fast signal propagation properties depend on the cathode and anode resistances. The anode wire resistance is about 60 Ω per metre for a DC current. For a real signal with a shaping time of 10 ns (25 ns at the base), the anode resistance remains the same due to the quite large skin depth of the Cu-Be wire (about 25 μm at 25 MHz).

The cathode resistance of the Kapton straw is about 400-800 Ω per metre long straw, and depends on the width of the tape from which the straws are produced. In the case of straws reinforced by carbon fibres, the propagation properties are improved due to the low resistance of the carbon fibres. The attenuation properties of these different types of straws were measured directly. It was found that for a signal with a shaping time of 10 ns, the attenuation length is 2-3 m (depending on the width of the tape) for straws without C-fibres and 4 m for straws with C-fibres.

We intend to use unterminated straw tubes. Their electrical connection to the front-end electronics is shown schematically in Fig. 3. The coupling capacitor (C_c) is shared between several (typically 4 to 16) straws which are connected to the HV through a HV resistor-fuse (R_{HV}), with a nominal value of 100 kΩ. This electrical chain is characterised by only one time constant, $T = R_{HV} \cdot C_c = 200$ μs. The discharge current of this chain goes through the input resistor of the preamplifier and has the same polarity as the fast signal from the straw. In case of straw breakdown, the fuse is designed to automatically disconnect the broken straw/wire from the I supply.

2.3 Operating properties of the straw tubes at LHC

2.3.1 Total signal collection time in a 2 Tesla magnetic field

At the LHC, the ATLAS TRT will be placed in a magnetic field. It is well known that the electron drift velocity in gases depends on the value of the magnetic field which generally leads to an increase in the total signal collection time.

Dedicated measurements of the drift velocity and Lorentz angles in a magnetic field of 2 Tesla were performed for the reference gas mixture of 70% Xe + 20% CF_4 + 10% CO_2. Preliminary experimental results [9] are shown in Figs. 4 and 5. The experimental data are compared with the results of simulations using the MAGBOLTZ program [10] for B = 0 and B = 2 T. Finally, the predicted drift velocity component, parallel to the electric field, which defines the total signal collection time, is shown in Fig. 6 for B = 0 and 2 T. This parallel component of the drift velocity is smaller in the magnetic field than that without magnetic field in the 1 mm region near the cathode (electric field less than 4 kV/cm). On the other hand, this component does not depend on the value of the magnetic field over the 1 mm region near the anode wire. The total collection time increases from 34 ns (B = 0) to 38 ns (B = 2T).

2.3.2 Straw counting rate due to charged particles and neutrons

Under LHC operating conditions, i.e. at the revised nominal design luminosity of 10^{34} cm^{-2}s^{-1}, the ATLAS straw tubes will be continuously irradiated by charged particles and neutrons. The charged particles are mostly minimum ionising particles. The straw occupancy, defined as the probability that the straw is hit in a given bunch crossing, depends on the radial position and length of the straw. In the worst case considered for operation at LHC (barrel TRT in ATLAS), the occupancy of the 1 m long straws is maximal for the innermost layer (R = 56 cm) and has been estimated to be 34%, assuming that one bunch crossing corresponds to an average of 18 minimum bias events. The corresponding occupancy in the endcap wheels is essentially independent of straw position, since the straws are radial, and is about 15%. This means that the maximum counting rate of the straws would be 14 MHz in the barrel part and 6 MHz in the endcap part.

The distribution of the neutron flux is quite uniform in the inner volume of LHC detectors. The total fluence of neutrons of all energies (including the thermal region) is around 10^{14} cm^{-2} per year. This gives a flux through the straw surface (50 x 0.4 cm^2) of 2 x 10^8 neutrons per second. Obviously, this flux will produce a certain rate of background signals in the straw tubes. The energy spectrum of the neutrons depends upon the detailed configuration of the detector system, in particular on the presence or the absence of a moderator. The primary flux consists of fast neutrons produced in the calorimeter, however, the presence of the moderator shifts this neutron energy spectrum towards the thermal region. To evaluate the neutron induced contribution of the straw counting rate, a dedicated measurement was performed, in operating conditions representative of those expected in ATLAS, including the moderator and the foam radiator surrounding the straws [5].

With a careful evaluation of the neutron flux from a ^{239}Pu-Be source, the probability for a neutron to induce a hit in a straw was found to be (0.9 ± 0.2) 10^{-3} for energy depositions less than 5 keV (corresponding to the expected energy loss of relativistic particles in the straws), and (0.4 ± 0.1) 10^{-3} for energy depositions of more than 5 keV (corresponding to the signals expected from transition radiation). These numbers include the contribution from photons due to (n, γ) reactions. For a normalised neutron flux of 10^{14} cm^{-2} per year of operation at LHC (pessimistic case), and a 50 cm straw length, Fig. 7 shows the estimated hit rates and occupancies from charged particles (a) and neutrons (b), for both of the above-mentioned energy deposition ranges. We conclude that the occupancy induced by the neutron background is an order of magnitude less than that due to charged particles.

2.3.3 Ageing properties of the straw tubes

The radiation hardness of the Kapton straw tubes and possible ageing effects have been widely investigated over the past few years [11, 12, 13, 14]. We limit ourselves here to the following remarks:

1. The radiation resistance of the Kapton straws is very high. No changes in the straws (gas gain, mechanical properties etc.) were observed for fluences of 4 x 10^{14} cm^{-2} from fast neutrons and of 1.7 x 10^{15} cm^{-2} from slow neutrons, and also for ionising particle doses of 80 Mrad. This is equivalent to more than 20 years of operation at the highest LHC luminosities.

2. No ageing in the straw tubes for a total integrated charge of up to 5 C/cm was observed, corresponding to over 8 years of operation at design luminosity.

3. No etching effects on the straw cathode were observed for a similar integrated charge. This was not the case for a thin unprotected Al-layer.

2.3.4 Space charge effects and straw performance at high fluxes of ionising particles

Due to the long drift time of positive ions in the straw tubes, some space charge is accumulated in the gas volume. In the worst case (first straw layers in the ATLAS barrel TRT), the intensity of charged particles per unit length is 14 MHz/40 cm = 3.5 x 10^5

particles per second. The ion space charge arising from such fluxes can change the electric field inside the straw. Dedicated measurements were performed to check the influence of this space charge on the gas gain and the drift-time accuracy. The experimental set-up was that used for the first straw drift-time accuracy tests (Fig. 8). Two straw tube arrays were placed one behind another in a beam of 2 GeV pions with a width of 15 mm. The straws were irradiated by an ^{55}Fe source (5.9 keV) up to intensities of 2.5 x 10^5 photons per cm per second, over a length of 22 mm, which covered the beam particle spread across the straws. The maximum total deposited charge was equivalent to a minimum ionising particle intensity of 7.5 x 10^5 particles per cm per second (assuming that the average energy deposition of charged particles in the straws is ~ 2 keV).

The time difference between signals from two consecutive straws was measured and used to extract the individual straw drift time measurement accuracy (~ 150 μm). Figure 9 shows the evolution of this accuracy and of the straw signal amplitude as a function of the intensity of straw irradiation. No deterioration of these fundamental straw properties was observed up to intensities of 6 x 10^5 particles per cm per second, i.e. about twice the LHC design luminosity.

One of the most serious problems for the design of the front-end electronics of straw tubes operating at high counting rate is the proper cancellation of the ion tails which contribute to the signal. Possible overlapping of ion tails from successive hits in the same straw may lead to a continuous but fluctuating current through the straw. This in turn causes base-line shifts in the electronic circuits and a resulting effective spread of discriminator thresholds. Techniques for eliminating such base-line shifts have been developed [15] but the inherent fluctuations may spoil the position accuracy of the straws, as obtained from drift-time measurements, and also give rise to fake hits and loss of efficiency. This means that a very precise cancellation of these ion tails has to be built into the front-end electronics. This item is now under detailed study and, in particular, an improved front-end preamplifier/shaper chip is under design.

The main operating properties of Kapton straw tubes at LHC are summarised in Table 4.

2.4 Conclusions

After several years of intensive research and development efforts, RD6 has reached the following conclusions on straw tube operation at LHC:

1. Kapton straw tubes of 4 mm diameter, reinforced with C-fibres, will operate reliably even at the highest LHC luminosities over a period of more than 10 years. The mechanical and electrical properties of these straws are now well understood and the specifications for the operation of a large straw tube system such as that proposed for ATLAS are now complete.

2. The straw tubes will operate reliably in a magnetic field, and their drift-time accuracy has been measured in test beam to be ~ 150 μ to 200 μ (see also Section 3.2), depending on the exact operating point and on the choice of front-end electronics. This performance has been shown to remain unaffected by the high local particle fluxes expected at LHC.

3. Fully assembled straw tubes have been thoroughly tested for resistance to radiation, both from ionising particles and neutrons, and also for possible loss of performance due to etching or ageing. With the chosen gas mixture and gas gain, no problem is expected for

more than 10 years of high luminosity operation at LHC. The occupancy induced by the high neutron flux expected in the central cavity has been measured and is expected to result in a relative increase of only 10% or less the straw occupancy from ionising particles.

4. Two items of concern remain and are under active study:
a) the impact of the large ion tails in the straw signals and of possible base-line fluctuations on the straw occupancy and drift time accuracy at high luminosity;
b) the evacuation of the heat dissipated in the straw gas volume by ionising particles.

3. Main results from 1991-1992 test beam data

3.1. General Detector Layout

The 1991-92 TRT prototype was tested at the H6 beam in the SPS from July to September 1991 and June to July 1992. In both runs, the set-up included scintillation counters for triggering, beam chambers for beam particle track reconstruction, a silicon pad detector for tagging of nearby charged particles (e.g. from photon conversion) and a prototype liquid argon calorimeter (RD3) which was used to reconstruct electromagnetic showers with good energy and position resolution.

The TRT prototype consisted of 4 blocks of 40 cm long straws embedded in a polyethylene foam radiator. Each block contained 24 rows of straws with 8 mm distance between rows and between straws within a row. The rows were randomly displaced with respect to one another to achieve uniform sensitivity of the detector, independently of the impact point and angle of incidence of the beam. The total thickness of the detector amounted to ~ 10% of a radiation length.

The straws were operated with a 70%Xe/20%CF_4/10%CO_2 gas mixture at a gas gain of ~ 10^4. This mixture combines the advantages of efficient TR-absorption, short drift-time and stability with respect to discharges. The total electron collection time was 34 ns. The Xenon concentration and the gas gain were carefully monitored throughout the run. The gas gain was stabilised by varying the operating voltage as a function of the ambient temperature and atmospheric pressure, using as a feedback signal the pulse height measured by sets of monitoring straws exposed to a ^{55}Fe source. The beam chambers were standard 400 μm resolution wire chambers, positioned at various distances along the beam line and allowing, together with the silicon pad information, reconstruction of the beam particle track.

The electronics used for this test consisted of preamplifiers mounted near the ends of the straws, connected to fast shaping amplifiers, which gave two signal outputs. The 'slow' output went to charge integrating analogue-to-digital converters (LeCroy 2282 Camac modules, 48 channels/module), and the 'fast' output went to fast discriminators with software programmable thresholds (Camac module designed at CERN, 24 channels/module). The latter were used to count TR-clusters, i.e. signals with energy above a pre-selected threshold. Only half of the channels (432 channels) were equipped with standard LeCroy time-to-digital converters (TDCs) for drift-time measurements. The data were treated by a CETIA/SD 6000 workstation, connected to a VME crate via an interconnect bus module. The target processor dedicated to real time tasks was a MC 68040 running a UNI/RT real time operating system.

During the 1992 run the performance of the prototype was also tested in the presence of a magnetic field. The set-up comprised the RD6 TRT prototype placed inside the ALEPH TPC90 magnet (a solenoid with magnetic field B = 0.78 T along the magnet axis, corresponding to a field transverse to the incoming particles of B_T = 0.257 T [16].

3.2. TRT tracking capabilities

3.2.1. Drift-time accuracy and alignment [17,18,19]

Figure 10 shows an event display of a 20 GeV pion in the TRT prototype. The upper part (straw hits) is presented on the same scale for both directions, whereas for the lower part (drift-time hits including left-right ambiguities) the scale of the vertical axis is magnified by a factor of 25. The drift-time to distance dependence is presented in Fig. 11 together with MC simulations using the drift velocity values taken from Fig. 6.

Fig. 12 shows in some detail how the expected drift-time accuracy per straw varies as a function of the straw discriminator threshold. Line 1 corresponds to a straw response simulation without any gas gain fluctuations and without electronic noise. Line 2 includes the effect of gas gain fluctuations. Finally, line 3 also includes the contribution from electronic noise, and is found to be in excellent agreement with the experimental data from the simple setup described in Section 2.3.4 and shown in Fig. 8.

In order to verify these first measurements with the large TRT prototype, using test be data in the magnetic field, a first necessary step is to align all the straw wires to an accuracy considerably better than 150 μ. Several alignment procedures have been studied using beam particles with and without the magnetic field, and comparing the results of a self-alignment procedure with those using external devices such as the beam chambers. In all cases, an iterative procedure was used, based on many independent data samples containing N beam particles. Both the anode wire position and the t_0 were fitted, assuming the same drift-time to distance relation for all straws (Fig. 11). After typically 6 or 7 iterations, stable values were obtained for the wire positions and t_0 -values, with a residual spread depending on N. A dedicated MC simulation of this procedure showed that the correct wire positions and t_0 -values are obtained, provided that there are no strong asymmetries in the distributions of tracks crossing the straws, especially in terms of left-right ambiguities.

The results are shown in Fig. 13 (B = 0) and 14 (B = 0.78 T), for beam particles of 20 GeV. In the case of Fig. 14, the incoming particle momentum was assumed to be known. Figures 13 and 14 show, for both the test beam data and the MC simulation, the alignment accuracy achieved as a function of N, using the beam chamber information (σ = 400 μ). With ~ 100 tracks per straw, an alignment accuracy of ~ 70 μ per straw is achieved. As shown in Figs. 13 and 14, this accuracy would improve to ~ 40 μ for an external track measurement accuracy of ~ 30 μ, as expected at LHC. Therefore, there seems to be no problem in measuring each wire position and t_0 value over a few days of low luminosity running at LHC.

Fig. 15 shows the drift-time residuals with respect to the fitted tracks before alignment (Fig. 15a) with σ = 250 μ and after the alignment procedure has been applied (Fig. 15b) with σ = 170 μ. This value is in reasonable agreement with the value expected from Fig. 12 for the straw discriminator threshold of 250 eV used in the test beam data.

3.2.2. Momentum resolution

Pion and electron beams of various energies were used to evaluate the momentum reconstruction accuracy of the TRT prototype in the magnetic field of 0.257 T transverse to the incoming beam particle direction. The reconstructed curvatures for pions and electrons of 20 GeV are shown in Figs. 16 and 17. The momentum accuracy is ~10% at 20 GeV, with some contribution expected from multiple scattering. A bremsstrahlung tail is clearly visible in the reconstructed curvature for electrons. Fig. 18 shows the measured σ_p/p as a function of p for the integral magnetic field value of ~ 0.32 T.m and for tracks traversing about 1 m of straw detector thickness. The slope of Fig. 18 at high momentum yields $\sigma_p/p^2 \sim 4\ 10^{-3}$, which can be roughly extrapolated to the ATLAS TRT in a magnetic field of 2T, resulting in an expected momentum resolution of $\sigma_p/p^2 \sim 8\ 10^{-4}$, i.e. 8% at 100 GeV for ~ 40 crossed straws and using a transverse vertex constraint (σ = 20 μ).

3.3. Single particle runs

3.3.1. Pion rejection [20]

The rejection against charged hadrons was measured using a 20 GeV hadron beam, which consisted mainly of π^+, and 30 GeV electrons to monitor the efficiency. The possibility of using the TRT for muon identification was investigated using muon beams with energy from 90 to 200 GeV. The dependence of the hadron rejection on various detector parameters such as the detector length, the angle between the straws and the beam, the gas composition and gain, the energy threshold for TR-clusters, the straw gain dispersion and the charge collection time was also studied.

Figure 19 [21] shows the differential energy spectrum expected per straw for 20 GeV pion data (dots) and for a detailed and dedicated simulation of dE/dx depositions [22] in the straws, including space charge effects, δ-electrons, energy resolution and relativistic rise. For 30 GeV electrons, Fig. 20 shows the comparison between the data and the above simulation, to which was added the contribution from transition radiation simulated for a regular-foil radiator [23]. The foam used in the data is of course not a regular foil radiator and this results in a reduced TR-yield (a factor 0.75 was applied to the MC-prediction to obtain the same rate of clusters with energy larger than 5 GeV) and in a slightly softer TR-spectrum in the data.

The energy threshold used to define transition radiation cluster candidates can be optimised in terms of hadron rejection at a fixed electron efficiency, typically 90%. The efficiency for 20 GeV pions as a function of this threshold is shown in Figs. 21a (B = 0) and 21b (B = 0.78 T). The optimum threshold is around 6.5 keV, but the curves do not vary much around this optimum, which means that a dispersion of 10-20% in overall straw gain from channel to channel does not deteriorate significantly the electron/pion separation.

We note that the pion rejection is about three times worse for B = 0.78 T than for B = 0 T. Careful investigation has shown that the apparent larger rejection without magnetic field is due to an increase in high-energy clusters by ~ 10% due to bremsstrahlung photons produced in the material upstream of the TRT prototype (~ 0.1 X_0), which initiate early showers in the straws themselves.

The distributions of the measured numbers of clusters with energy above 5.5 keV are shown in Fig. 22 (30 GeV electrons) and Fig. 23 (20 GeV pions), for a 70% Xe gas mixture and a typical angle of 63º between the straws and the beam particles.

Using pion, muon and electron beams of different energies, the yield of TR-clusters has been accurately measured as a function of $\gamma = E/m$, as shown in Fig. 24. The threshold dependence needs to be understood, since the ATLAS TRT tracker will provide a level-2 trigger for $J/\psi \to e^+e^+$ decays for $p_T^e > 1$ GeV, a threshold close to the lower limit for good electron/pion separation with a standard transition radiation detector.

3.3.2. Rejection of photon conversions in the absence of magnetic field [20]

The rejection of photon conversions was studied with the same set-up as the one described above. A beam of 150 GeV electrons went through a 0.08 X_0 Pb-converter. The electron beam was subsequently deflected by a magnet towards the upper part of the LAr calorimeter without traversing the other detectors, while the produced bremsstrahlung photons with their characteristic 1/E spectrum went through two converters upstream of the TRT and triggered the apparatus if their energy was above 20 GeV. The first converter was 2 mm Al (2.2% X_0), placed 300 cm upstream, and the second was 10 mm CH_2 (2.1% X_0), 70 cm upstream.

These two converters were installed to simulate closed conversions, i.e. electron pairs not seen as two separate tracks in the straw prototype, and open conversions or Dalitz decays, i.e. electron pairs often reconstructed as separate tracks in the straw prototype. These two categories were selected off-line, using the silicon pad detector in front of the TRT prototype which selected closed conversions as events where only one pad was hit with a pulse height compatible with that from two minimum ionising particles, and open conversions as events where only two silicon pads were hit, each with a pulse height compatible with that from one minimum ionising particle.

As an illustration of the behaviour of such events in the TRT prototype, as compared to electrons, the distributions of N_{12} (number of straw hits with energy between 0.2 keV and 1.5 keV) versus N_3 (number of TR-hits with energy larger than 5.5 keV) are shown in Fig. 25a (electrons), 25b (closed conversions in front of the TRT prototype) and 25c (conversions inside the straw prototype itself). As expected, N_3 is about twice as large for closed conversions in front of the TRT as for electrons, and the situation is observed to be intermediate for the internal conversions.

Table 5 compares, for a 90% electron efficiency, the rejection factors which were obtained against closed and open conversions as a function of photon incident energy. When two tracks from very asymmetric conversions are reconstructed in the TRT prototype, the TR-response is approximately the same as for single electrons, which explains the better rejection achieved against closed conversions than against open conversions. Finally, a rejection of 0.039 ± 0.001 was obtained against internal conversions, for events with a reconstructed TRT track.

3.4. Target run: performance in a high multiplicity environment

The TRT prototype was also tested behind a target, used to simulate the high occupancies expected from pile-up at LHC design luminosity. The whole detector set-up was positioned for this run at an angle of 40 mrad below the direction of the incoming beam particles. A mixed pion/proton beam of 205 GeV energy interacted in a thin Be-target situated 70 cm before the TRT. The trigger was based on a coincidence between a large amplitude observed in a scintillator counter behind the target and a shower of at least 10 GeV energy in the LAr calorimeter behind the TRT.

The display of one such triggered event is shown in Fig. 26. By superimposing on top of such events, events from the single particle runs, an experimental measurement of the TRT performance in a high multiplicity environment was obtained. A robust and simple track reconstruction was used in order to minimise the sensitivity of the results to systematics in the track finding procedure: a road of $\pm$ 3 mm width with respect to the known single particle direction was scanned in fine angular and position steps to find the best track candidate, defined as the one maximising the difference between the number of crossed straws with a hit above threshold and the number of crossed straws without a hit.

Figure 27 shows, as a function of the straw occupancy and for an electron efficiency of 90%, the pion and photon-conversion rejections obtained with this procedure. The straw occupancy is defined from the target run data above as the fraction of straws hit within a road of ± 1 cm around the reconstructed track. Fig. 28 shows the measured distribution of this occupancy in the target run data, which reaches values well above the highest straw occupancies foreseen in ATLAS at LHC.

For the occupancy values expected at LHC design luminosity (20% average occupancy in the ATLAS barrel TRT and 15% in the endcaps), the photon conversion rejection is unaffected, whereas the pion rejection is worse by an order of magnitude than at very low occupancy. Of course, more detailed simulations have been performed to properly take into account the different correlations in a magnetic field.

The impact of high occupancy on the TRT track reconstruction capabilities was also studied using the target run data. As shown graphically in Fig. 26, roads with widths of ± 1 cm were investigated in terms of fake track reconstruction as a function of their angle θ_{FAKE} compared to the average angle of the real tracks θ_{REAL} originating from the target. Figure 29 shows the distributions for three different values of θ_{FAKE}-θ_{REAL}: 100 mrad (a), 50 mrad (b) and 10 mrad (c). These average values of θ_{FAKE}-θ_{REAL} correspond to different degrees of correlation between the hits from the real track and those from the fake track direction. For small values of θ_{FAKE}-θ_{REAL}, the correlation is the greatest and corresponds to pattern recognition inside high p_T jets. For the ATLAS TRT at LHC in a magnetic field of 2 T and for the average p_T of 0.3 GeV of minimum bias tracks, the average value of θ_{FAKE}-θ_{REAL} is much larger, approximately 1 rad.

Figure 30 shows the dependence of the fake track probability on θ_{FAKE}- θ_{REAL} using the target run data and MC for extrapolation to the case of LHC. This figure demonstrates that the TRT pattern recognition capabilities remain quite robust even at the highest LHC luminosity, provided that the number of crossed straws per track remains close to 40.

3.5. Backsplash Studies [24]

One of the problems wich may arise when trying to realistically describe the straw occupancy might be the backsplash rate in the inner detector from the electromagnetic calorimeter, which comprises a high material density and therefore a high backsplash probability. Although it affects mostly electromagnetic interacting particles (e, γ), any significant deviation from the MC prediction may underestimate the occupancy in the outermost tracking layers.

Using the TRT prototype, this backsplash probability was measured using a lead brick, positioned ~ 5 cm behind the TRT prototype, in order to maximise any backsplash effects. Data were taken to study in particular the behaviour of the backsplash from the lead brick, depending on the energy of the incoming particle, the particle type (e,π), the angle between the particle and the brick surface and the magnetic field. In order to understand the sensitivity to some of the MC simulation parameters, the energy spectrum of hits outside the direction of the incoming particles, which consist mainly of δ-electrons and backsplash particles, was studied.

Every feature due to the backsplash which was visible in the experimental data was also qualitatively found in the MC simulation. From the quantitative point of view, no discrepancy was observed between the MC and the data in the absence of backsplash. However, in the case of maximum backsplash, i.e. for a brick angle of 45º, for B = 0.78 T and for 60 GeV electrons, twice as many backsplash hits were observed in the data as compared to the MC prediction (see Fig. 31).

This discrepancy, although large, does not have any serious implications for LHC, since the predicted backsplash occupancy from low energy minimum bias tracks is much smaller than the occupancy due to the tracks themselves.

4. TRT in ATLAS

The TRT has been fully simulated within the ATLAS inner detector , as shown in Fig. 32, and the most recent results are summarised in the latest ATLAS documents to the LHC Committee [25,26]. We briefly summarise here the performance figures most relevant to the TRT.

4.1 Straw occupancy and TRT pattern recognition

Despite the high values expected for straw hit probabilities at LHC design luminosity, typically 15-20%, the straw tracker as such provides a very robust tracking performance due to several factors [27]:

a) the straws are equipped with drift-time measurement. Although multiple hits will reduce the effective single-straw efficiency (since the wrong time may be assigned to a hit), the track search uses roads tuned to the drift-time bins. Given the measured drift-time accuracy of ~ 150-180 μm, such a bin has a width of ± 300-400 μm. The occupancy of these bins is typically three times less than the straw hit probability. This results in a 5-10% effective single straw occupancy in the ATLAS TRT.

b) The probability of finding a fake track depends on the number of measurement layers and on possible correlations between the background hits. With ~ 40 hits per track, the fake track rate is negligible in the case of random background hits. Hits from low momentum particles, as expected for minimum bias events, have no strong correlation in the 2 T magnetic field when searching for high-momentum tracks.

c) In some cases a looping track, or a coincidence of several low momentum tracks, may produce a very high local occupancy (see for example Fig. 33). Since the straws are evenly spread over a large radial range, high-momentum tracks can still be detected with high efficiency in the unaffected regions.

Figure 33 shows the hits produced by the overlap of 40 minimum bias events, corresponding to a luminosity of 1.7 x 10^{34} $cm^{-2}s^{-1}$, in the barrel TRT as a function of azimuth. Five electrons and five muons of 20 GeV energy have been superimposed on top of this hit pattern. Histograms of the number of normal hits, E > 0.2 keV (right), and of high-energy hits, E > 5 keV (left), are shown as a function of azimuth for each part of the barrel TRT (L1 and L2) and for the total barrel (L1+ 2). This example shows that high p_T tracks can be distinguished easily in the pattern of hits even at such high luminosities, and that such a histogramming technique will provide an easy-to-implement and reliable level-2 track trigger.

All the above arguments are quantified in Fig. 34 which shows the probability to find a fake track in a typical level-1 trigger road defined by a calorimeter cluster or the muon system as a function of luminosity. It can be seen that for transverse momenta above 15 GeV, the number of fake tracks is an order of magnitude less than for real pile-up tracks at the design luminosity, if the drift-time information is used. We note, however, that the relevant figure of merit is given in Fig. 34 by the expected level of real electrons after the level-1 trigger rejections has been applied.

Figure 34 thus shows that the TRT level-2 track trigger performance will be adequate at the highest LHC luminosities even without using the drift-time information.

4.2 Evaluation of TRT performance for B-physics

As part of the simulation work required to study the ATLAS capabilities for B-physics, an unbiased sample of $B_d^0 \rightarrow J/\psi K_s^0$ decays was generated, fully simulated and reconstructed [26]. These events contain a muon tag with $p_T > 6$ GeV and $|\eta| < 1.6$ (staged muon trigger system), two charged leptons with $p_T > 1$ GeV and $|\eta| < 0.8$ from J/ψ decay, and two charged pions with $p_T > 0.5$ GeV and $|\eta| < 0.8$ from K_s^0 decay. The K_s^0 decay radius R_d was required to satisfy 1 cm < R_d < 50 cm for reasons of background (lower cut) and fiducial volume (higher cut).

Figure 35 shows, for luminosities L of 1 x 10^{33} (left) and 5 x 10^{33} $cm^{-2}s^{-1}$ (right), a transverse view (R-ϕ plane) of one of these events with a $J/\psi \rightarrow e^+e^-$ decay and a K_s^0 decay with $R_d \sim 40$ cm. One half of the ATLAS barrel tracker is displayed with the hits in the straw tracker (the straws cover the range $0 < \eta < 0.8$) and in the semi-conductor layers, where the hits are summed over the same η-range. To account for the different luminosities, two (left) and ten (right) minimum bias events have been added on top of the signal events in Fig. 35. The tracks with $p_T > 0.5$ GeV reconstructed using a global pattern recognition algorithm based on the straw tracker itself, are shown as dotted lines between the detector planes. For both luminosities considered, all the interesting final state particles have been reconstructed and are indicated by full lines and labelled with particle type and reconstructed p_T.

These events have been used to evaluate the capabilities of the ATLAS inner detector to reconstruct K_s^0 decays and in particular $B_d^0 \rightarrow J/\psi K_s^0$ final states as a function of luminosity. The global pattern recognition algorithm reconstructs with high efficiency all tracks, including secondaries, with $p_T > 0.5$ GeV and with at least two precision measurements (in both R-ϕ and z) in the silicon layers at radii of 50 and 80 cm in addition to the straw tracker hits. All pairs of oppositely charged particles with a distance of closest approach, d_{min}, smaller than 5 mm are then considered as V^0-candidates, if the decay radius R_d is within 1 cm < R_d < 50 cm. Figure 36 shows the K_s^0 mass resolution (left) and reconstruction efficiency (right) as a function of R_d for three different K_s^0 transverse momenta (3, 5 and 7 GeV) typical of $B_d^0 \rightarrow J/\psi K_s^0$ decays. Over most of the decay radius range the mass resolution is 3-4 MeV. The K_s^0 reconstruction efficiency includes the track reconstruction efficiencies, the cut $d_{min} < 5$ mm used to validate a pair of oppositely charged tracks as a V^0-candidate, and the cut on $m_{\pi^+\pi^-}$ used to define the V^0-candidate as a K_s^0 candidate. The drop in efficiency at small values of R_d for a K_s^0 p_T of 3 GeV is an artefact of the fiducial cuts used to define the barrel tracker acceptance. The drop in efficiency at large values of R_d and large values of the K_s^0 p_T is mainly due to the straw tracker two-track resolution. The average efficiency is 91% and the background contamination under the K_s^0 peak is only 6% with these very loose cuts. At the higher luminosity, L = 5 x 10^{33} $cm^{-2}s^{-1}$, the K_s^0 reconstruction efficiency drops to 88% and the background under the peak increases to 11%. This excellent performance in reconstructing secondary decay vertices is largely due to the continuous straw tracker.

If needed, tighter cuts may be applied to define K_s^0-candidates, as illustrated in Fig. 37 for K_s^0 transverse momenta of 3, 5 and 7 GeV. Shown as a function of R_d are the expected measurement precisions for the decay radius R_d (top left), the minimum distance d_{min} (top right), the K_s^0 impact parameter and the longitudinal position of the K_s^0 trajectory on the beam line. Most of these quantities can be measured quite accurately, to better than 1 mm for $R_d < 30$ cm and tighter cuts using these quantitites improve the signal to background ratio considerably.

In terms of the ATLAS physics reach in studies of CP-violation in B-decays, this performance of the ATLAS tracker, studied using a full simulation of the complete inner detector, is crucial both for level-2 triggering on specific B-decays and for signal reconstruction and background rejection. For example, the ATLAS detector is expected to measure the parameter $\sin 2\beta$ with an accuracy of $\pm$ 0.03 for an integrated luminosity of 10^4 pb^{-1}. Both the straw tracker capabilities and the transition radiation performance of the ATLAS TRT are expected to play a major role in this performance.

5. TRT prototype status

5.1. TRT sector prototype

The TRT sector prototype is designed to be positioned inside the ALEPH-TPC 90 magnet, and consists, as shown in Fig. 38, of radial straws distributed over a 30º azimuthal sector (endcap geometry of the ATLAS TRT). The main purpose of this prototype is a systematic study of the TRT performance in a configuration where both the detector and the electronics (see Section 6) are as close as possible to those foreseen for ATLAS. Due to the limited space inside the magnet, the straw length had to be reduced to 33 cm, as compared to 50 cm in the endcap ATLAS TRT. The total length of the prototype is 90 cm and the ionising beam particles will cross the straws with an angle of ~ 70º. This corresponds to a pseudorapidity of 1.8 in the ATLAS TRT. Therefore 20 GeV energy beam particles will produce a hit pattern similar to that of 50 GeV energy tracks in the ATLAS geometry at η = 1.8 (due to the different magnetic fields of 0.78 T and 2 T).

The full sector prototype consists of 6 blocks each containing 512 straws. Each block of 32 radial straws is placed inside a support frame with an accuracy of ~ 100 μm. The edges of the frames are constructed so as to provide a common gas manifold for all the straws and the necessary electrical connections. The inner part of the frames was constructed out of carbon fibre composite material, in order to minimize the radiation length. The total averaged radiation length of this inner support, including the straw endplugs, is about 1.4% X_0 for normal incidence. All frames inside of two blocks are fully equipped with straws and the gas gain uniformity has been measured to be better than 5%. The gas tightness of the full system is good enough to operate with a gas flow of 0.05 cm^3/min per straw. Sixteen polypropylene foils of 15 μm thickness and spaced by 230 μm are used as a radiator between the frames. The front-end electronic chips (see Section 6) are connected to printed boards on the outer radius of the frames.

Two full blocks of the sector prototype, containing 1024 straws, are now under test in the H8 beam, and a full test with the complete system is planned for May 1994.

5.2. Full-scale engineering prototype of one endcap module for the ATLAS TRT

The purpose of this second prototype is to assess the mechanical feasibility of a full-scale endcap TRT module. During 1992 and the first half of 1993, a complete and detailed design of this prototype has been made (figure 39 shows a schematic view of this module). Major constraints on the mechanics arise from the need for light and radiation resistant materials. This has led to the concept of a 134 mm long module with 16 planes of 600 straws. The straws have a length of 500 mm and a diameter of 4 mm. In order to achieve a good uniformity for the number of crossed straws for tracks with $p_T > 0.5$ GeV, each plane of straws is rotated in azimuth by a fraction of the distance between two consecutive straws.

Figure 40 shows the connection of the straws and the radiators to the inner and outer rings. The radiator material between the straw planes is made of a stack of 12 sheets of polypropylene of 14 μm thickness, spaced by 300 μm gaps. As discussed in Section 2.1, the straws are made of Kapton foils: Kapton, as all plastics, is known to creep under load. But, in addition to creep and thermal expansion, tests have shown that humidity modifies considerably the mechanical behaviour of the straws. Two approaches have been studied to solve these environmental problems:

- maintaining the straw under constant tension through the use of a spring-like device connected to the straw outer end;
- stiffening the straw itself.

The latter option has been preferred: each straw is rigidified by 4 strands of 1000 filament carbon fibre glued along the straw axis. While the straw rigidity is multiplied by a factor larger than 20, the extra material increases the probability of X-ray absorption by only 20%. In addition to producing stiffer and straighter straws, the forces exerted on the supporting structure by the straws and their wires are smaller, leading to the possibility of using even lighter materials. This is particularly important for the inner wheel (diameter 1 m) and also for the end flanges of the ATLAS barrel TRT.

The radial straws are mounted between two concentric rings made of light composite materials. Extensive structural analysis has shown that under normal loading, all the deflections will remain below 100 μm. Both rings have been manufactured and delivered by industry (Fig. 41):

- the 1 metre diameter inner ring made of Kevlar fibres in epoxy resin weighs only 1.454 kg (the winding tool weighs more than 1 ton !);
- the 2 metre diameter outer ring, which is the stiffest part of the structure, is made of high-module carbon fibre in epoxy resin and weighs 4.982 kg.

Each wheel was accurately drilled with 9600 holes used to fix the straws. The global accuracy (tolerances on hole diameter and position) for these 9600 holes is of the order of 20 μm. Qualification tests under mechanical loads have shown the very good quality of the manufacturing and an excellent agreement (better than 5%) with the expected behaviour.

All the plastic connection parts (mechanical or injected) and the 50 μm diameter CuBe wire have been delivered and the assembly of the prototype has begun in a dedicated hall. In parallel, systematic radiation tests (up to 10^7 Gy) are being performed in order to qualify all the components of the structure. The full prototype is expected to be ready for tests in spring 1994.

5.3 Design studies and construction of a barrel prototype

Most of the RD6 efforts in terms of hardware have concentrated until now on the enormous task of building the large prototypes discussed above with a radial straw geometry for the endcap ATLAS TRT.

In the barrel region, a different geometry has to be adopted, using longer axial straws embedded in a foam optimised for transition radiation production. Because of this some R&D work has to be done in order to establish the TRT technique in this region for ATLAS:

a) Detailed studies of straw response for one metre long straws. This work is already in progress and it seems that the signal propagation properties of longer reinforced straws will be adequate for reliable operation at LHC with the same front-end electronics as for the 50 cm long straws;
b) R&D on foam materials for transition radiation production. This work is also in progress both for boron-based foams and for a promising polyethylene-based commercial foam;
c) Design of a small prototype with 2 m long split axial straws embedded in the chosen foam. This design would only address the mechanical problems specific to this geometry, in order to establish as quickly as possible the viability of the technique through the production of a small prototype;
d) Investigations are under way to understand whether thin and small honeycomb cells could be used in this geometry;
e) Extensive design work with the goal of integrating the barrel TRT into the ATLAS inner detector. System aspects, such as alignment, service routing, cooling, integration of different mechanical structures, are of paramount importance in this area.

RD6 plans to progress as much as possible along these avenues of research in the coming year.

6. TRT electronics and triggering

6.1. Concept of readout electronics

The TRT readout needs to record the status of two thresholds, a low one for the minimum ionising particles and a high one for the TR photons. In addition, the TRT measures the track coordinate from the drift time (DTM). For this purpose the time elapsed between the beam crossing and the low threshold discriminator transition is measured. The method of the phase locked loop is used to automatically link the time measurement to the phase of a master clock (BX) (Fig. 42). The DTM provides 3 bits of information, corresponding to an rms error of about 1 ns (equivalent to 45 μm).

The task of the electronic readout system is to store the threshold and DTM information during the level-1 trigger latency, to record it in a local memory upon reception of a level-1 trigger (T1) and to transmit it to the level-2 trigger processor and to the readout buffer. If a valid level-2 trigger occurs, the data will then be further processed and stored by the data acquisition system (DAQ).

A general overview of the system is given in Figs. 43, 44, 45. The front-end electronics for 32 straws are implemented on a printed-circuit board (daughter-board DB) directly mounted onto the detector. 16 DBs, serving 512 straws are connected to a supervisor module ('digital readout electronics'), which coordinates data transfer to the level-2 trigger processor and to DAQ, distributes BX and T1 and controls the status of the derandomiser on the front-end. The supervisor module also transmits the slow digital signals controlling the thresholds to the front-end.

All components of this system, designed early in 1992, are now completed and tested. The DTM logic is soon going into production and will be available by May 1994.

6.2. Analogue front-end electronics

The analogue front-end consists of an amplifier, a shaper and two discriminators. The amplifier is designed to give 2000 electrons of noise when connected to a straw of 15 pF capacitance. The shaper is designed to give Gaussian-like pulses with a peaking time of 8 - 10 ns and a width of 20-25 ns at the base.

The analogue front-end for a group of eight straws is implemented on an ASIC made in bipolar technology (TRDA). The DC voltages defining the thresholds are supplied externally and are thus common to all eight channels. The spread of the comparator offsets of the individual channels inside a chip is smaller than the noise. All output signals of this chip are differential current pulses. The power consumption of the TRDA is 100 mW (about 13 mW/channel). The DC voltages defining the thresholds are produced by a control chip (TRDC). This chip also converts the differential current pulses from the TRDA to CMOS and passes them to the digital delay line, which is the next element of the readout chain. The CMOS pulses could of course have been produced in the TRDA itself. There was serious concern, however, that unipolar logic pulses would crosstalk to the amplifiers, inhibit low threshold operation and limit the efficiency for minimum ionising particles. The control chip also contains a test pulse option and the logic interface to the slow control.

6.3. Digital front-end electronics

The information on thresholds and DTM, corresponding to 5 bits per straw, is stored into a digital pipeline working at the beam crossing frequency to allow a level-1 trigger latency of about 3 μs. Upon reception of each level-1 trigger, the information of 3 subsequent bunch crossings is stored in a memory which can accommodate the data of up to 5 events (derandomiser). These functions together with some logic for the control of the DAQ are all integrated in one CMOS chip, the readout controller (ROC). The ROC consumes 120 mW running at 40 MHz (4 mW/channel). A set of four TRDA, four TRDC and one ROC are mounted on the DB. Data transfer between the DB and the supervisor module occurs via differential current signals. This is regarded as a precondition for high digital noise immunity of the discriminator operation.

6.3.1. Status of the readout

All units mentioned above are tested and operational. Measurements of the noise level of the input across the whole readout chain - but with the straws yet unconnected - show the expected low level of front-end noise. This observation is interpreted as an experimental confirmation of the design goal of negligible digital-to-analog interference on the DB.

6.3.2. Future plans

The work on the TRT electronics will proceed with the following priorities:

a) test of a system of several thousand straws in the H8 beam:
   - efficiency for minimum ionising particles
   - e/π separation
   - level-2 trigger processor operation
   - stability of the readout system at high level-1 trigger rate (10^5 Hz)

b) implementation of the drift-time measurement
   - measurement of drift-time accuracy in the test beam

c) study of radiation-hard processes
   - the present implementation of the digital chips, TRDC and ROC in CMOS is not radiation-hard. Alternative technologies will be investigated.

d) other tasks
   - readout by optical fibres
   - reduction of power consumption at the front-end
   - reduction of the size of the front-end elements and of the board.

6.4. Front-end electronics based on SAW delay lines

A front-end electronic system based on surface acoustic wave (SAW) technology has been considered as a possible alternative to the present front-end electronics design.

The principle of SAW operation is based on the propagation of acoustic waves on a pie:-electric crystal surface. The electrical signal is transformed into an acoustic wave which propagates with a velocity of about 3000 m/s (for $LiNbO_3$ crystals). The delay time is defined by the geometrical size of the crystal, typically a delay time of 1 μs for a 3 mm crystal. The overall delay time accuracy which can be achieved in modern technology is better than 1 ns. A specimen of an 8-channel SAW front-end electronics element was designed and produced using semi-custom integrated chips. The signal after amplification and shaping is modulated by a 200 MHz carrier wave and goes to the SAW delay line, which delays the input signal by (2 μs + 60 ns x i), where i is the channel number. All 8 channels are then multiplexed into a serial output buffer.

Full testing of the SAW delay line electronics connected to the straws is planned for the end of 1993.

6.5. Level-2 triggering with the TRT

One of the important characteristics of the TRT is its capability of using both its tracking and particle identification in real time. Together with RD11, several pilot implementations are under way to demonstrate this capability and evaluate the constraints on the front-end electronics imposed by a level-2 trigger system.

Level-2 triggering with the TRT has to be implemented within the constraints of a maximum level-1 trigger rate of 50 to 100 kHz. Data are stored in the front-end electronics until the level-1 trigger broadcasts its decision, a fixed time ('latency') after the bunch crossing in question. If the trigger decision is 'yes', a transfer of all TRT data to the level-2 buffer takes place. If not, the buffer will simply be freed for overwriting.

A fraction of these data, indicated by an η-ϕ pointer found by the level-1 trigger will be used for decision taking. This fraction covers a coherent geometrical area of the TRT called a 'region of interest' (RoI). An RoI is estimated to correspond to about 1% of the total TRT data. Several RoIs may be flagged for a given level-1 trigger.

It is the task of the TRT trigger to extract an RoI, and to convert the data contained in it to relevant physics-related parameters needed for decision making. This process is called 'feature extraction', and reduces substantially the amount of data passed onto subsequent (trigger-internal) steps. In the case of the TRT, the features are tracks (if found) and their geometrical parameters (η, ϕ, p_T), together with an electron flag using the high threshold data. Multiple RoIs give rise to multiple feature extraction operations that can run in parallel. In further processing, the extracted data (features) are combined with those of other detectors, first for the same RoI and then for the full set of data in order to extract a global level-2 decision.

During the October-November 1993 beam tests, RD6 will for the first time provide an LHC detector prototype operating with front-end electronics with LHC functionality. It is intended to trigger the system at 100 kHz level-1 rate, so that both data transmission and level-2 triggering can be tested at full speed. The implemented trigger will demonstrate a data selection unit ('Router') and two alternatives for the conversion of TRT raw data to track parameters ('feature extraction'). All units tested will demonstrate execution of the triggering algorithm at 100 kHz or faster, so that no event parallelism is required.

The Router tested in RD6 is a synchronous unit reading all raw data for several events into a multi-port memory. The unit passes information without affecting the data acquisition and selects, guided by a level-1 trigger pointer, a rectangular region in ϕ/Z for transmission to the feature extraction processor. To ease processing, simple local format changes in the data are made, and the order of the data is changed; both are programmable operations.

Two feature extraction devices will be connected to the Router: one is a commercial image processing system (Max Video), the other is a custom-designed systolic array based on Xilinx programmable gate arrays, called Enable. Max Video has prewired special and parallel processors for operations like convolutions, windowing, table lookup, or morphological transformations. All run on a data pipeline of 20 MHz (8 or 16 bits). The internal switching between these units is fully programmable, and so are all coefficients for transformations. For the purpose of the TRT track finding algorithm, the system is used to histogram data in the ϕ/Z plane along straight lines of different slopes or p_T. The Enable machine executes an algorithm very similar to that of Max Video, but has a TRT-adapted parallelism which makes it superior in performance and scalability. Enable executes its algorithm by comparing the data to stored bit patterns rather than straight lines, so that a data 'warping' operation (non-linear transformation of the coordinate space) can be easily programmed.

As shown in Fig. 46, the planned test makes the trigger operation a simple data intercept invisible to the data recording system except for the possibility of reading the trigger results. All external communications are via HIPPI cables, chosen to be a suitable, if temporary, high-band width standard.

7. Milestones for 1994, test beam requests and budget estimates

7.1 Milestones and sharing of responsibilities

During 1994, RD6 expects to take the final steps towards demonstrating the functionality of the TRT (mechanics, electronics and system aspects) for ATLAS at LHC:

a) completion of assembly and tests of full sector prototype (MEPHI, Lebedev, Dubna);
b) upgraded and complete front-end and readout electronics, including the implementation of drift-time measurements (CERN, RAL/Glasgow, Lund, MPI, Krakow, PNPI);
c) extensive tests in the H8 beam (52 days in total), including a complete test of level-2 triggering in collaboration with RD11 (all institutes)
d) assembly and test of full-scale engineering prototype (CERN, MEPHI, Lebedev);
e) barrel prototype design and construction (Aachen, CERN, Lund, MEPHI, Siegen);
f) study of high-rate performance of straws (Lebedev, Lund, MEPHI, MPI, RAL/Glasgow, PNPI);
g) further simulations for optimisation of TRT performance in the ATLAS inner detector (CERN, MEPHI, Lebedev).

7.2 Test beam and computer time requests for 1994

We request 52 days in the H8 beam over three periods in May, August and September 1994, for a complete evaluation of the full sector prototype (3000 straws) in a magnetic field. During these periods, we will study:

a) Tracking properties;
b) e/π separation;
c) Electron-positron pair reconstruction ability in the magnetic field;
d) Drift-time measurements with the new readout system;
e) Level-2 trigger implementation studies (together with RD11).

We also plan to complete the analysis of the 1992 data and fully analyse the first batch of 1994 data. For this reason, we request a total of 2000 hours on the CERN IBM for 1994.

7.3 Budget estimates

CERN budget request (kCHF)

a.	Assembly and test of the full scale engineering prototype	90
b.	Straw and component production for barrel prototype	50
c.	Test beam run	70
d.	Upgraded electronics for sector prototype	110
		sub-total 320

Lund budget request (kCHF)

a.	Barrel prototype design and construction	130
b.	Upgraded FE-electronics: implementation of DTM	40
		sub-total 170

Moscow (MEPHI and Lebedev) budget request (equivalent kCHF)

a.	Prototype sector completion	20
b.	R&D on foam for barrel prototype	15
c.	Production of kapton film for the barrel straws	15
d.	TRT high-rate performance tests	15
		sub-total 65

RAL/Glasgow budget request (kCHF)

a.	Upgraded FE and readout electronics	20
b.	High-rate FE electronics studies	10
		sub-total 30

MPI budget request (kCHF):

a.	Upgraded FE electronics, including the implementation of the DTM	45
b.	High-rate FE electronics studies	15
		sub-total 60

Siegen University budget request (kCHF)

Barrel prototype design and construction **50**

PNPI budget request (equivalent kCHF)

High-rate FE electronics developments, production and tests **10**

JINR (Dubna) budget request (equivalent kCHF)

Sector prototype completion **50**

Krakow budget request (kCHF)

Front-end and readout electronics tests **10**

Aachen budget request (kCHF)

Electronics for sector prototype and barrel prototype studies **10**

Acknowledgements:

We are very grateful to the RD3 Collaboration for allowing us to work with the Liquid Argon Accordion Calorimeter, and for their help in adapting their data acquisition system to our needs. We wish to express also our gratitude to the RD11 and RD13 Collaborations for their help in preparing the level-2 trigger and DAQ systems for our test beam run.

We thank K. Bussmann and G. Di-Tore for their continuous contributions for the preparation of mechanics and electronics for the test beam runs. We also thank participants from Boston, BNL, CERN, Krakow and MEPHI for their various contributions to this project.

References:

[1] V.A. Polychronakos et al., Integrated high rate transition radiation detector and tracking chamber for the LHC, CERN/DRDC/90-38 (19.08.90).

[2] V.A. Polychronakos et al., Integrated transition radiation and tracking detector for LHC, CERN/DRDC/91-47 (22.10.1991).

[3] ATLAS Letter of Intent, CERN/LHCC/92-4, LHCC/I2 (01.10.1992).

[4] ATLAS Collaboration, The ATLAS Inner Detector, Status Report, CERN/LHCC/93-24.

[5] ATLAS Internal Note INDET-No-18; V. Bondarenko et al., CERN-PPE/92-171.

[6] Moscow electronics group, RD6-Note, 10 April 1992.

[7] I. Iljuschenko, The electrical model of the straw chamber, RD6-electronics meetings, 21.01.93.

[8] D. White, RD6-Note-17 (1991).

[9] J. Hiddleston, N. McCubbin, V. Sosnovtsev, to be published; RD6 Collaboration meeting, April 1993.

[10] S.F. Biagi, Nucl. Instrum. and Methods, A283 (1989) 716.

[11] V. Bondarenko et al., Nucl. Instrum. and Methods, A327 (1993) 386.

[12] V. Bondarenko et al., CERN-PPE/91-191 (1991).

[13] V. Bondarenko et al., RD6-note 35, 20 October 1992.

[14] M. Carpeans et al., CERN-PPE/93-136 (1993).

[15] The straw group, SDC-note, 23 May 1993.

[16] N. Zaganidis, Technical Note RD6, 4 June 1992.

[17] V. Bashkirov, I. Gavrilenko, S. Schuh, RD6 Technical Note 32.

[18] S. Schuh, Vorbereitungspracticum aus KERN und Teilchenphysik LV-Nr. 142.285.

[19] W. Fuchs, RD6 Note 43.

[20] M. Stavrianakou, PhD Thesis, 1993.

[21] P. Nevski, ATLAS Internal Note, to be published.

[22] V. Ermilova et al., NIM, 145 (1977) 555.

[23] G.M. Garibian, Zh. Eksp. Teor. Fiz. 33 (1957) 1043; Sov. Phys. JETP 6 (1958) 1079.

[24] W. Funk, ATLAS Internal note, to be published.

[25] Progress Report on ATLAS milestones, CERN/LHCC/93-51, 15 October 1993.

[26] B-physics with the ATLAS experiment at LHC, CERN/LHCC/93-53, 15 October 1993.

[27] I. Gavrilenko, ATLAS internal note, INDET-No-016.

Table 1: Mechanical properties of Kapton straw tubes

Diameter	4 mm
Wall thickness	60 μm
Young's module of straw material	300 kg/mm^2
Relative elongation at 200 g load	10^{-3}
Temperature coefficient of elongation	3×10^{-3} per °K
Anode wire diameter (Cu-Be)	50 μm
Anode wire tension	50 g

Table 2: Mechanical properties of reinforced straw tubes

Number of carbon fibres	3 or 4
Relative elongation at 200 g load	6×10^{-5}
Temperature coefficient of elongation	3×10^{-6} per °K

Table 3: Electrical properties of the straw tubes

Cathode conductive layer	2000 Angs. Al + μm C-loaded Kapton
Resistance of the conductive layer	3 - 5 Ω per square
Cathode resistance (for a one metre long straw)	400 - 800 Ω
Anode wire resistance (for a one metre of 50 μm Cu-Be wire)	60 Ω
Skin depth for Cu-Be alloy at 25 MHz	25 μm
Capacitance of assembled straw for one metre length	20 pF
Anode wire inductance	1600 nH
Straw impedance $\lvert Z_0 \rvert$ (measured at 30 MHz)	300 Ω
The best passive termination	300 - 330 Ω
Signal attenuation length: without carbon fibres with carbon fibres	 2 - 3 m 4 m
Signal propagation time	4 ns/m
Signal parameters (point source): Short straw (less than 50 cm) 1 m long straw at far end 1 m long straw at near end	Gaussian shape: 24 ns at the base 26 ns at the base 28 ns at the base

Table 4: Operating properties of the straw tubes

Gas mixture	70% Xe + 20% CF_4 + 10% CO_2
Gas gain	2.5×10^4
Nominal high voltage	1780 V
Total collection time for electrons for B = 2 T	38 ns
Total collection time for ions	60 μs
Time constants of ion current $t < 120$ ns $120 < t < 350$ ns $t > 350$ ns	 59 ns 5 ns 9.5 ns
Electron contribution to the signal amplitude for a shaping time of 10 ns	50%
Signal uniformity along the straw	Better than 5% r.m.s. for straws of 1 m length
Signal uniformity for different straws	Better than 10% for 1 m length or less
Maximum tolerable counting rate	6 $\times 10^5$ particles/cm/s
Max. current pulse for 6 keV at a gas gain of 2.5×10^4	10 μA for a shaping time of 20 ns at the base
Max. continuous ion current at highest LHC luminosities	7 μA
Max. power dissipation in gas	13 mW
Ageing Etching	more than 5 C/cm (8 years at LHC) more tha.n 2.5 C/cm (no traces of etching seen)
Straw radiaiton resistance	Fast neutrons: up to 4×10^{14}/cm^2 Slow neutrons: up to 1.7×10^{15}/cm^2 Dose from charged particles: 80 Mrad
Minimum gas flow needed through the straw	0.05 cm^3/min per straw

Table 5: Rejection of photon conversions versus photon energy

Energy GeV	ε_{closed}	ε_{open}
0 - 25	0.060 ± 0.004	0.137 ± 0.009
25 - 50	0.030 ± 0.003	0.084 ± 0.008
50 - 75	0.023 ± 0.003	0.073 ± 0.011
75 - 100	0.013 ± 0.003	0.064 ± 0.013
100 - 125	0.013 ± 0.003	0.073 ± 0.016
125 - 150	0.011 ± 0.003	0.073 ± 0.022

Table 6: Sharing of responsibilities and funding for 1994

Institution	Full sector prototype production	Upgraded FE electronics	Test beam in 94	Engineering wheel prototype	Barrel prototype	High rate TRT performance	MC simulation TRT in ATLAS	Total kCHF
CERN		110	70	90	50		+	320
Lund		40	+		130	+		170
Moscow (MEPHI + Lebedev)	20		+		30	15	+	65
RAL/Glasgow		20	+			10		30
MPI		45	+			15		60
Siegen			+		50			50
PNPI			+			10		10
JINR (Dubna)	50		+					50
Krakow		10	+					10
Aachen		10						10
Total kCHF	70	235	70	90	260	50		775

+ Participating institute
All requests subject to approval from relevant funding authorities

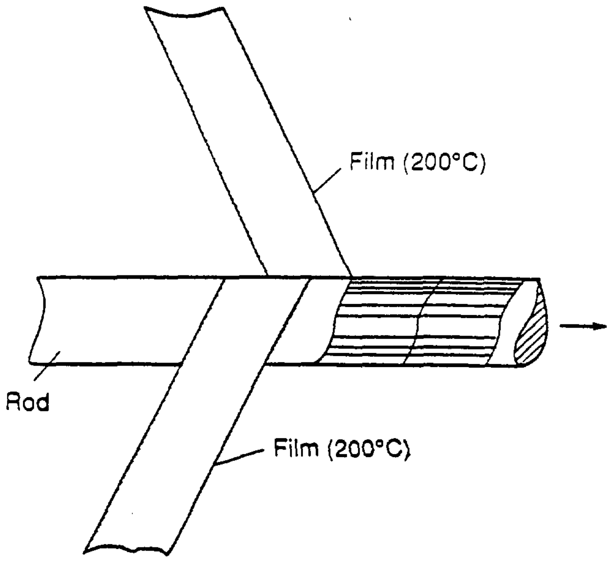

Fig. 1 The straw manufacturing procedure.

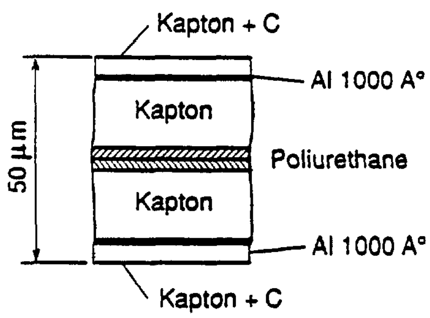

Fig. 2 Cut through the straw wall.

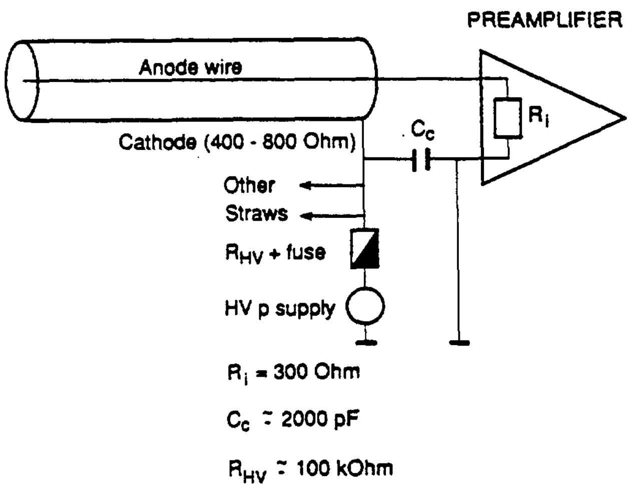

Fig. 3 Electrical connection of straw to HV supply and preamplifier.

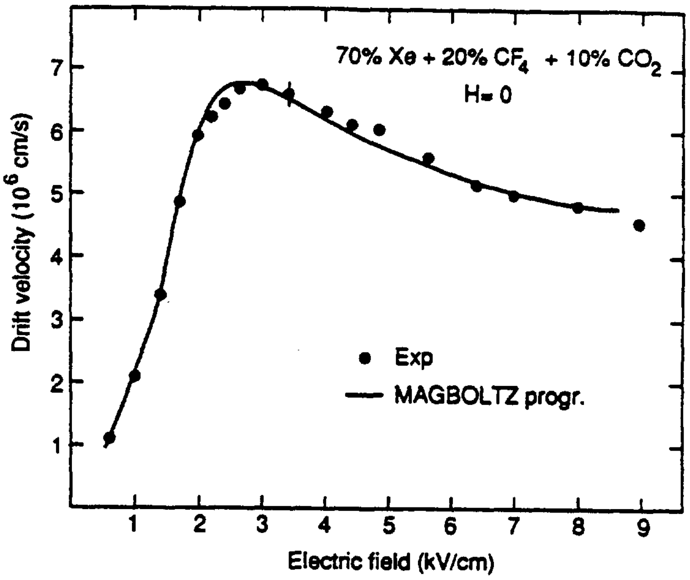

Fig. 4 Drift velocity of electrons versus electric field: data and predictions for B = 0.

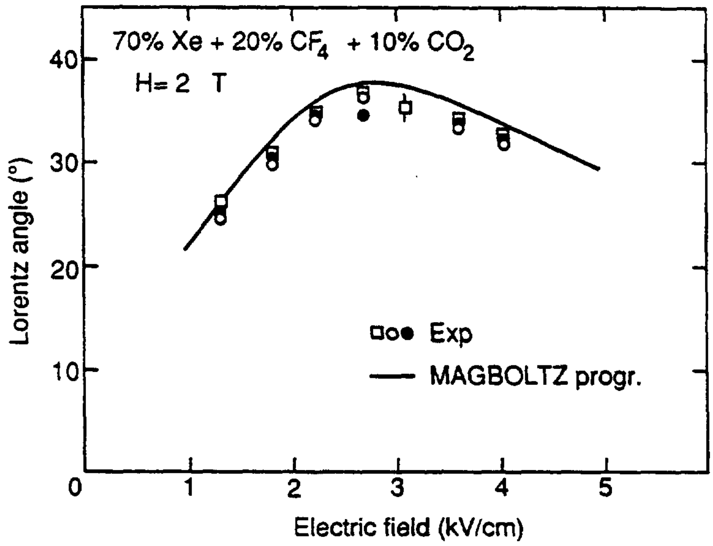

Fig. 5 Lorentz angle versus electric field for B = 2 T: data and predictions.

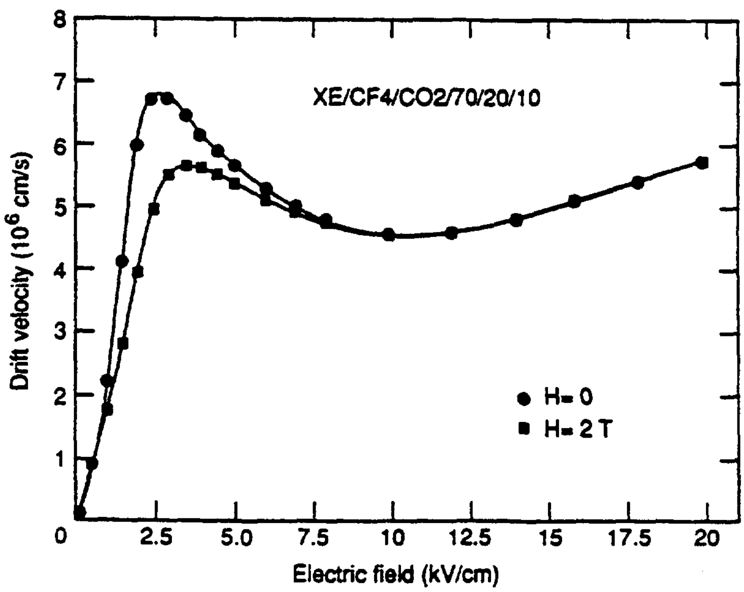

Fig. 6 Predicted drift velocity component parallel to electric field for B = 0 and B = 2T.

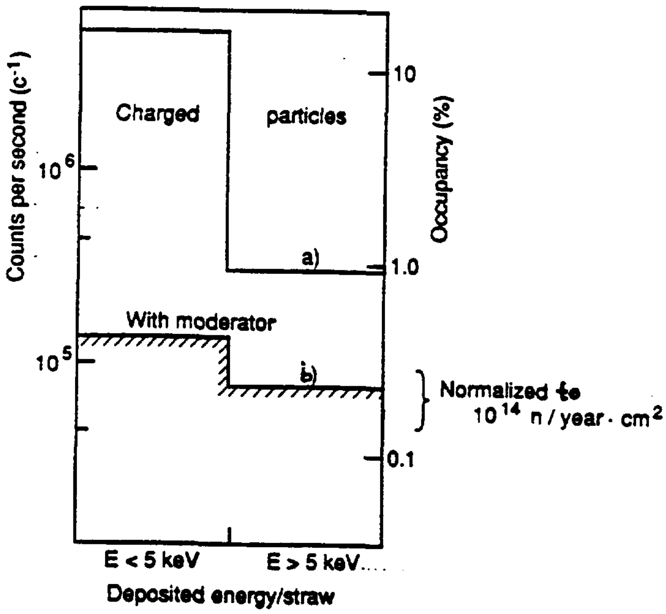

Fig. 7 Rate and occupancy of straws induced by charged particles and by neutrons (including photons) for a luminosity of 1.7×10^{34} cm^{-2}s^{-1}.

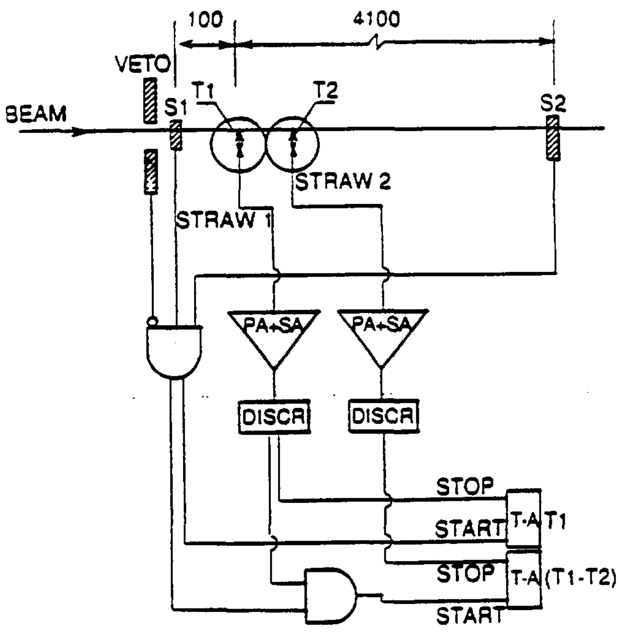

Fig. 8 Experimental set-up for the measurements of the straw drift-time accuracy.

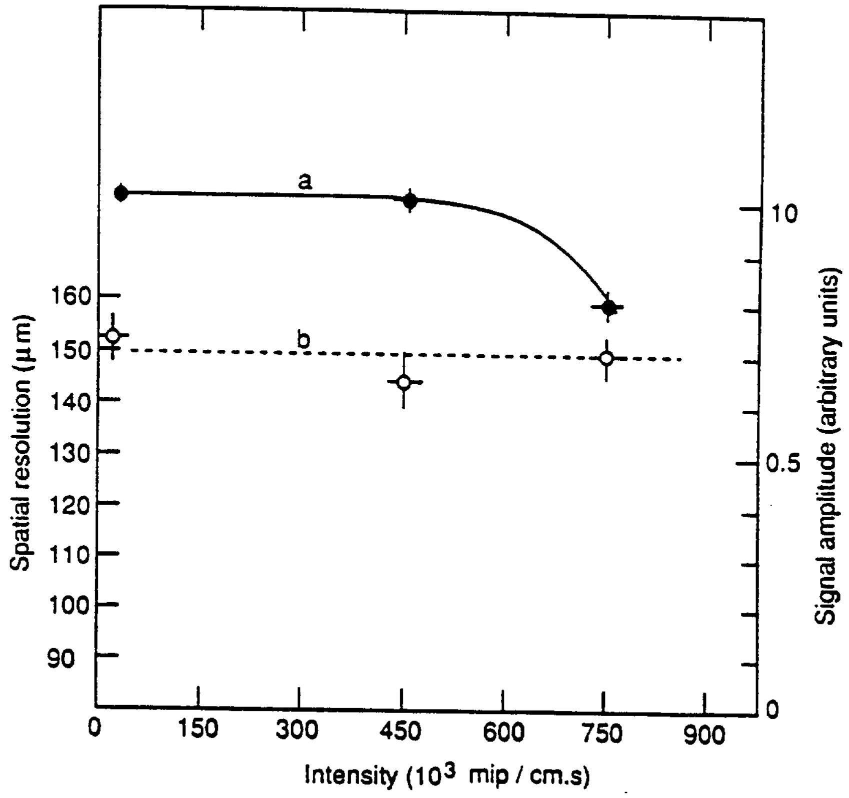

Fig. 9 Amplitude of the signal from ^{55}Fe (a) and drift-time accuracy (b) as a function of charged particle rate per unit straw length.

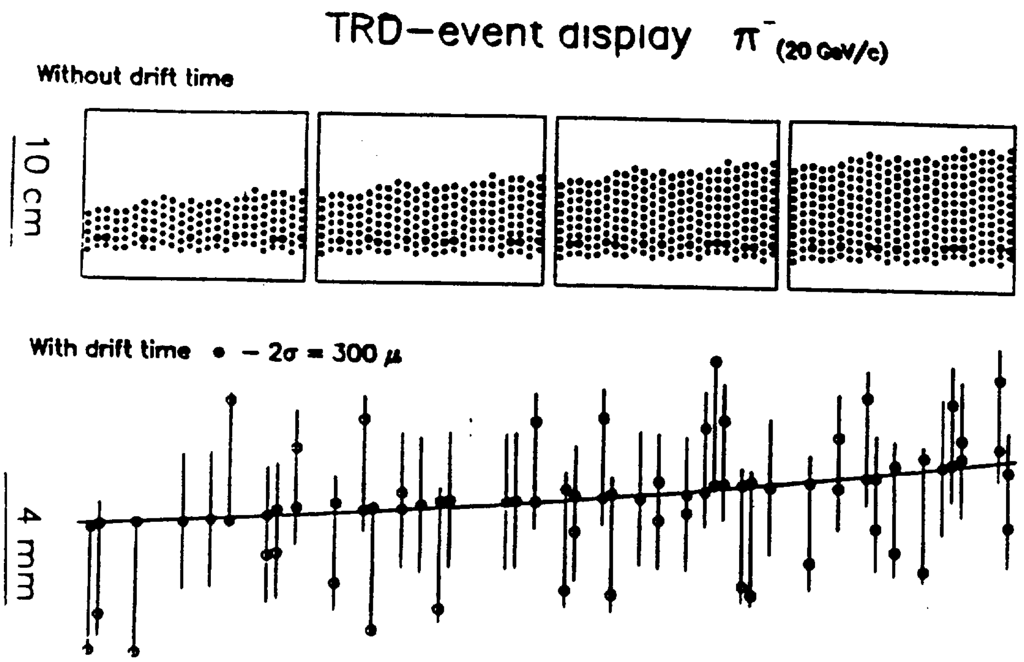

Fig. 10 TRT-prototype event display for the 1992 run in a magnetic field. The lower part corresponds to the drift-time hits with a magnification of 25 along the vertical axis.

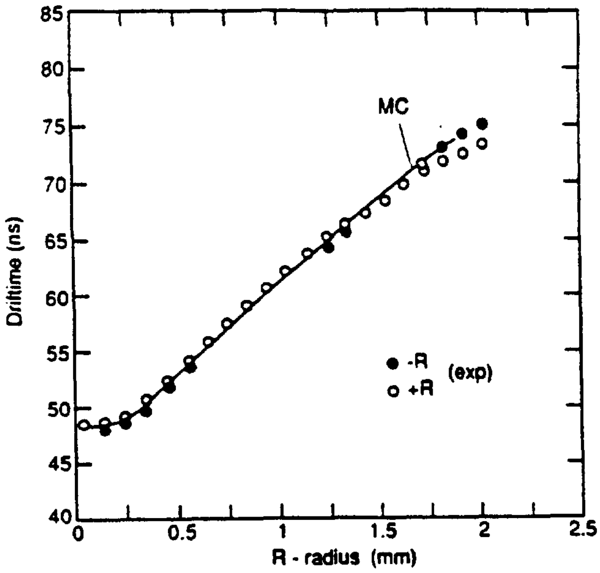

Fig. 11 Measured and predicted drift-time to distance relation in a straw.

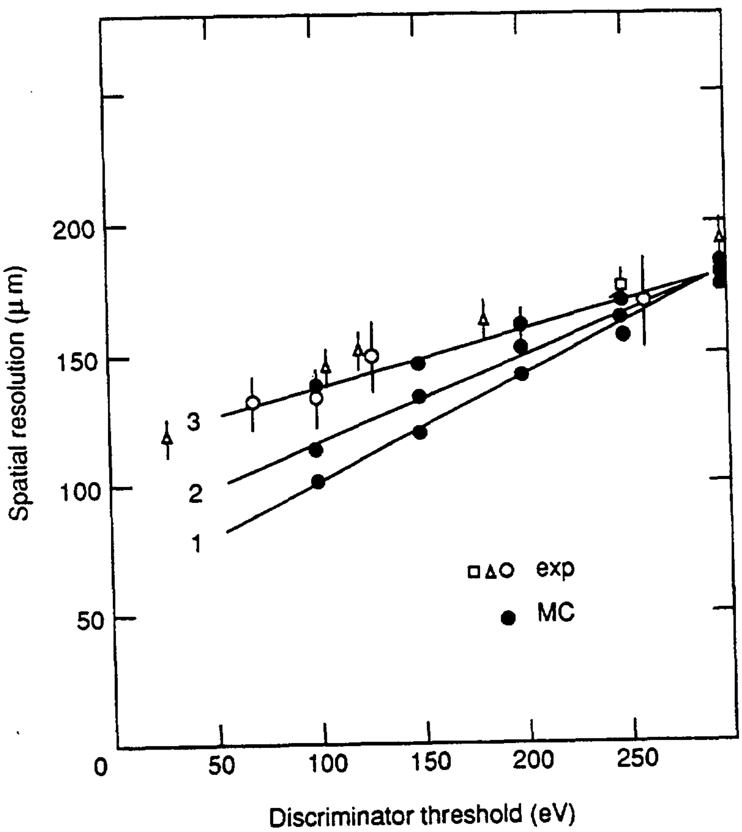

Fig. 12 Comparison, as a function of threshold, of drift-time accuracy measurements with MC model without gas gain fluctuations and without electronic noise (1), without electronic noise (2) and with both electronic noise and gas gain fluctuations (3).

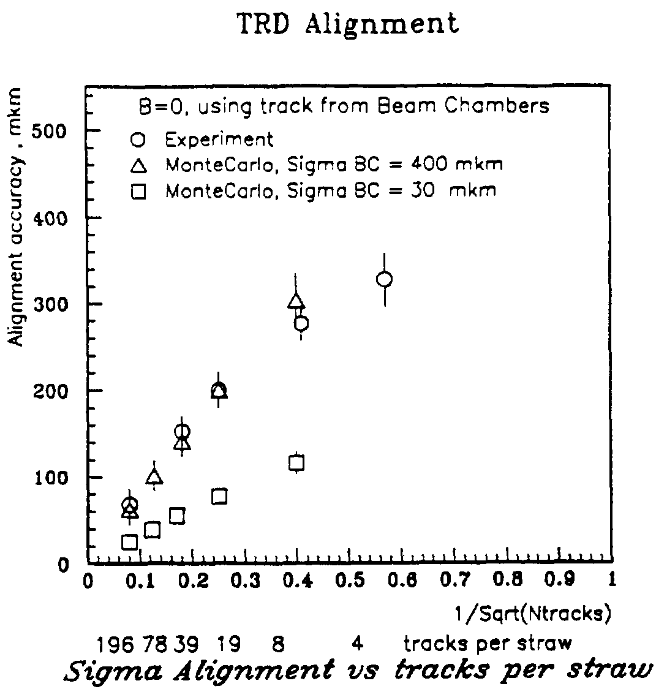

Fig . 13
Accuracy of straw wire alignment as a function of $1/\sqrt{N}$ for B = 0, where N is the number of beam particles used.

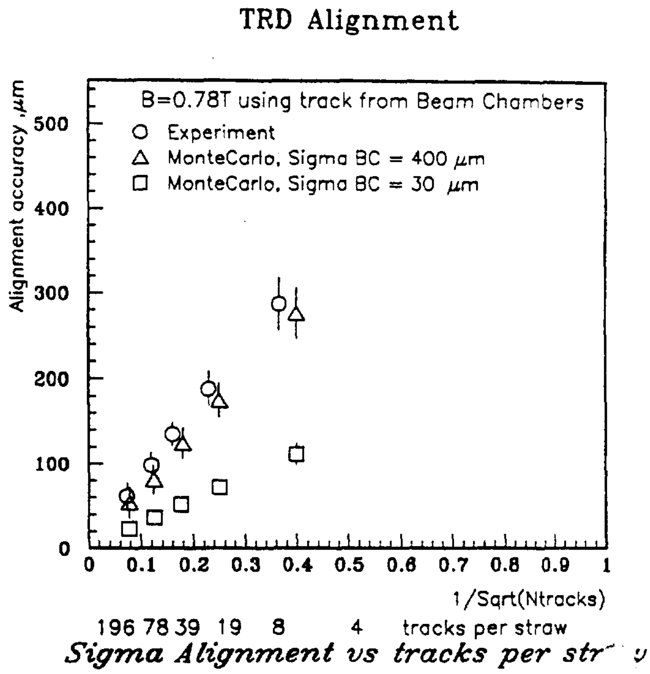

Fig. 14
Accuracy of straw wire alignment as a function of $1/\sqrt{N}$ for B = 0.78 T, where N is the number of beam particles used.

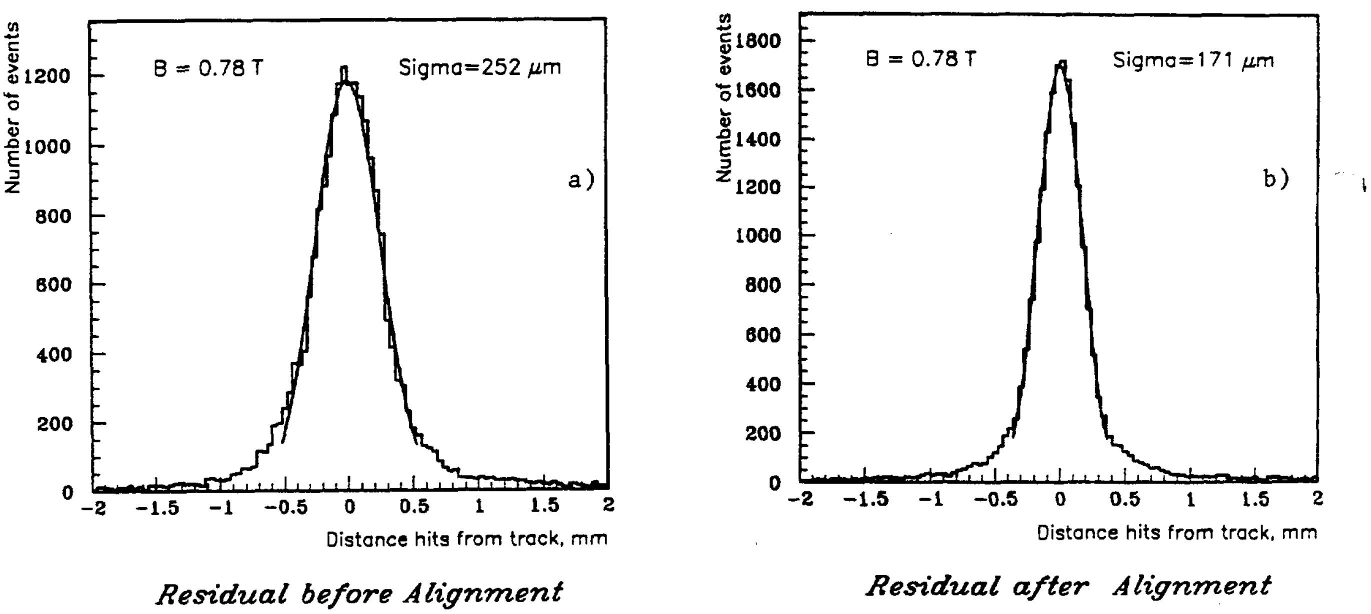

Fig. 15 Wire residual distributions before alignment (a) and after alignment (b) for B = 0.78 T.

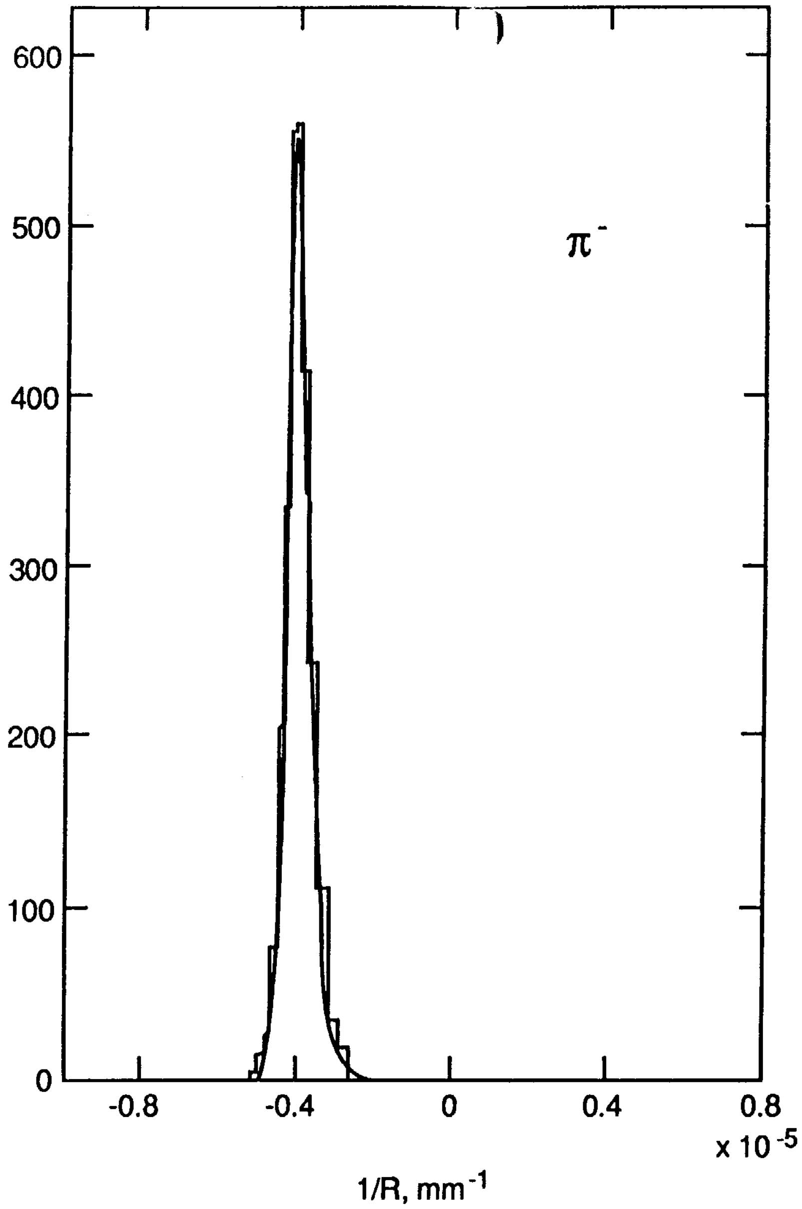

Fig. 16 Accuracy of curvature measurement for 20 GeV pions and B = 0.78 T.

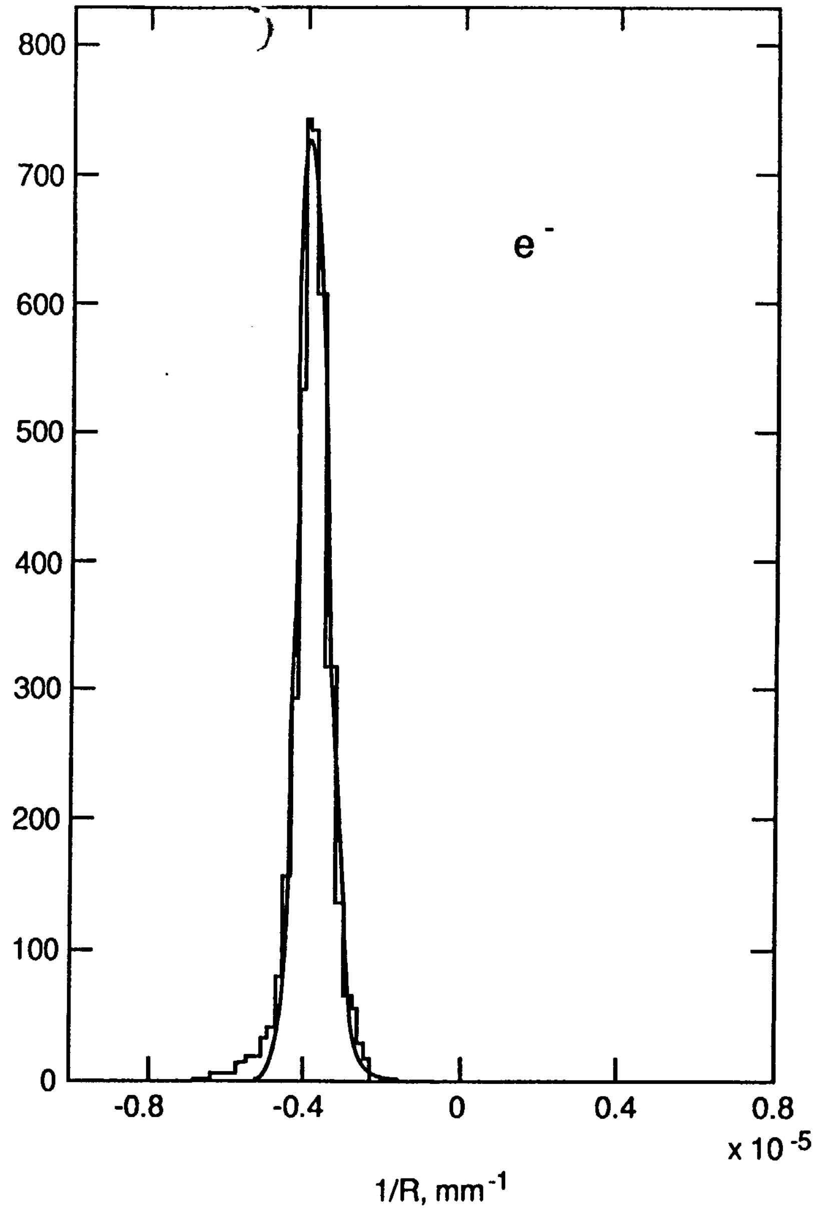

Fig. 17 Accuracy of curvature measurement for 20 GeV electrons and B = 0.78 T.

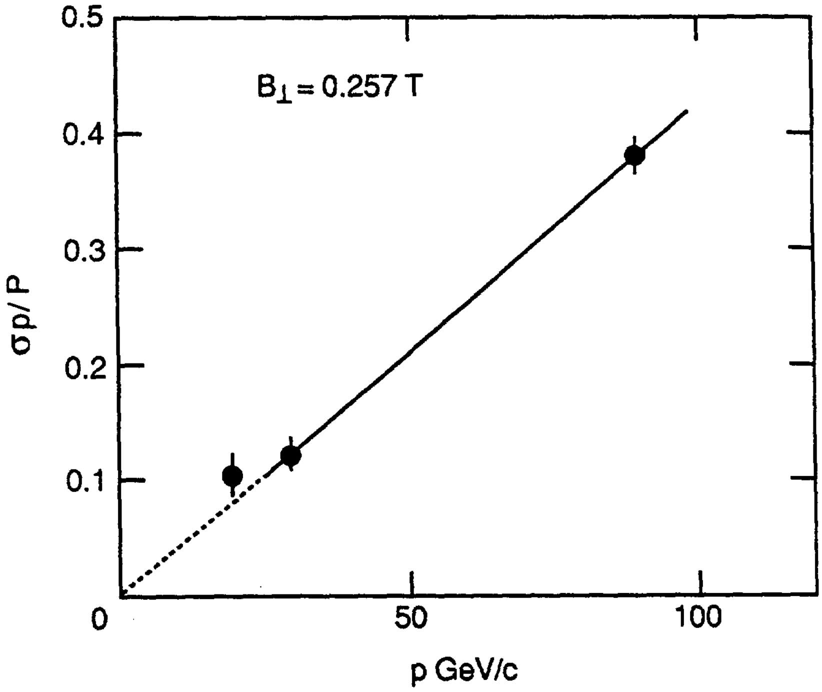

Fig. 18 Momentum resolution versus reconstructed momentum for B = 0.78 T.

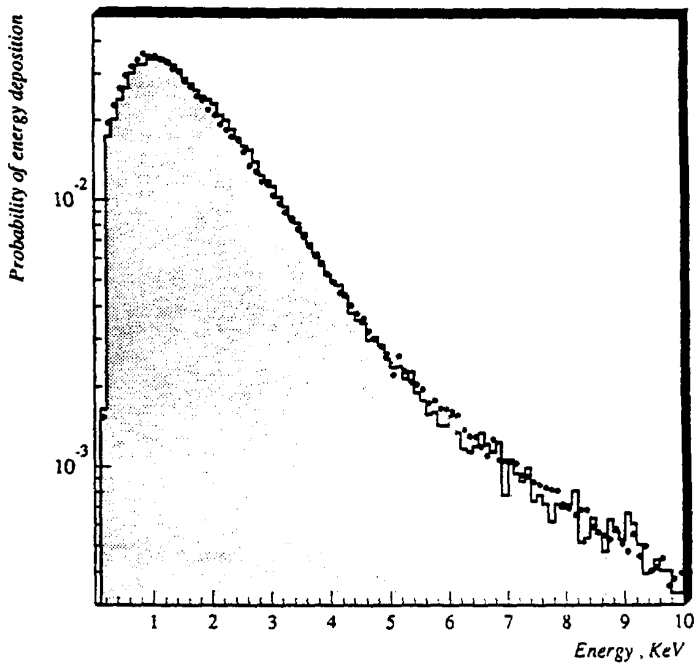

Fig. 19 Differential distribution of hit energies measured for 20 GeV pions (dots), compared to a detailed MC simulation (solid line) of straw response.

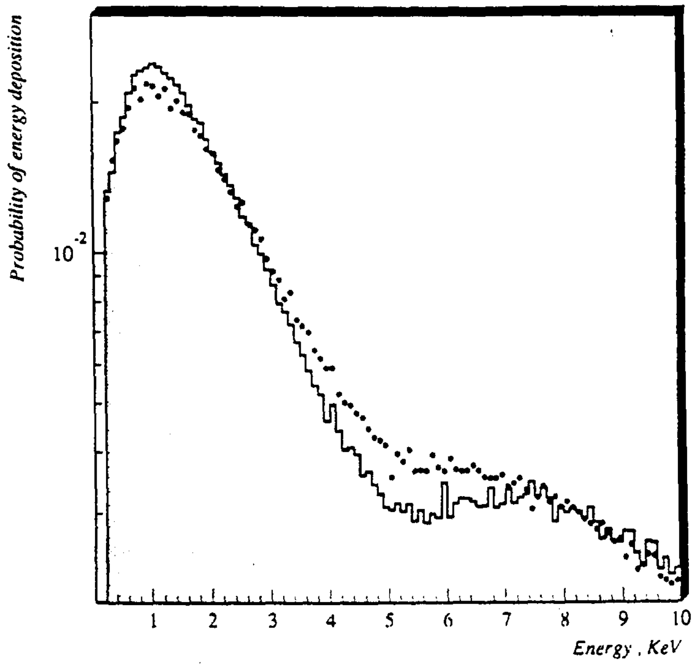

Fig. 20 Differential distribution of hit energies measured for 20 GeV electrons (dots), compared to the MC simulation (solid line) including dE/dx and TR-production/absorption.

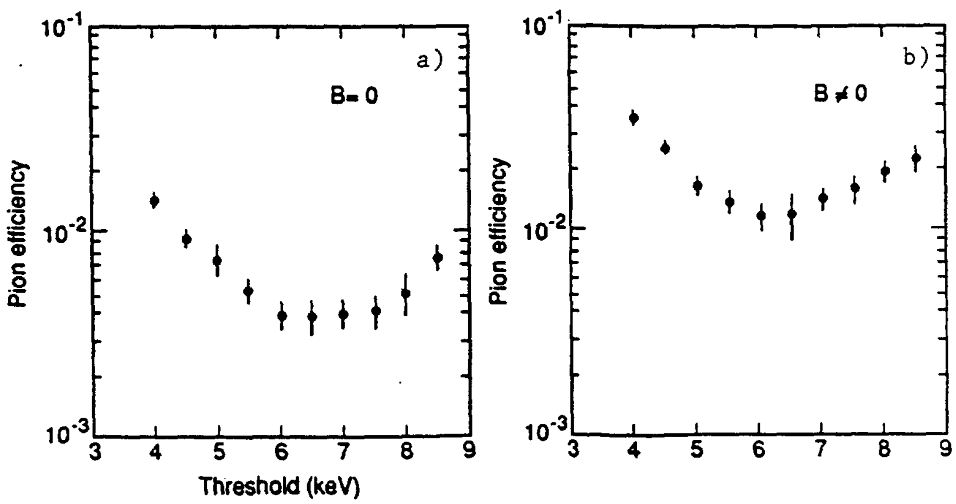

Fig. 21 Optimisation of energy threshold for TR clusters for B = 0 (a) and B = 0.78 T (b).

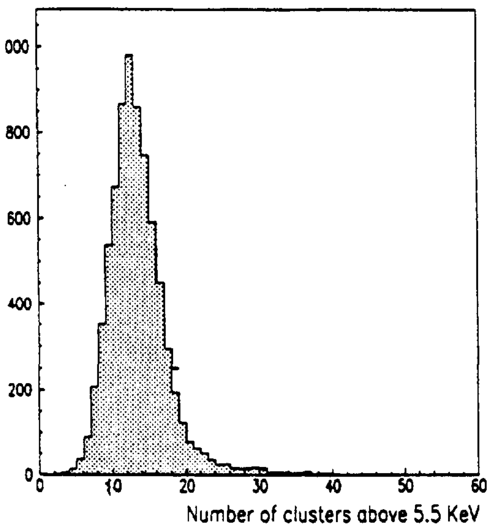

Fig. 22
Distribution of number of clusters with energy above 5.5 keV for 30 GeV electrons.

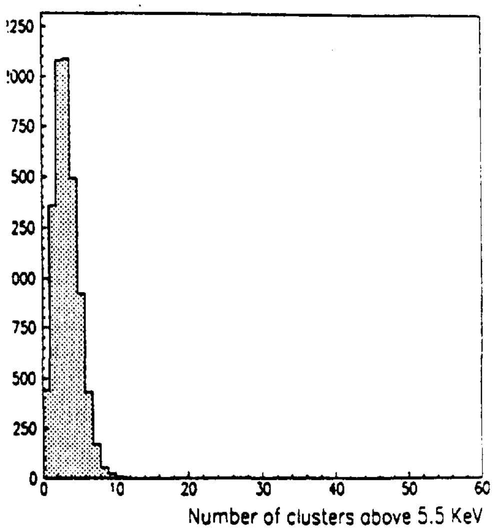

Fig. 23
Distribution of number of clusters with energy above 5.5 keV for 20 GeV pions.

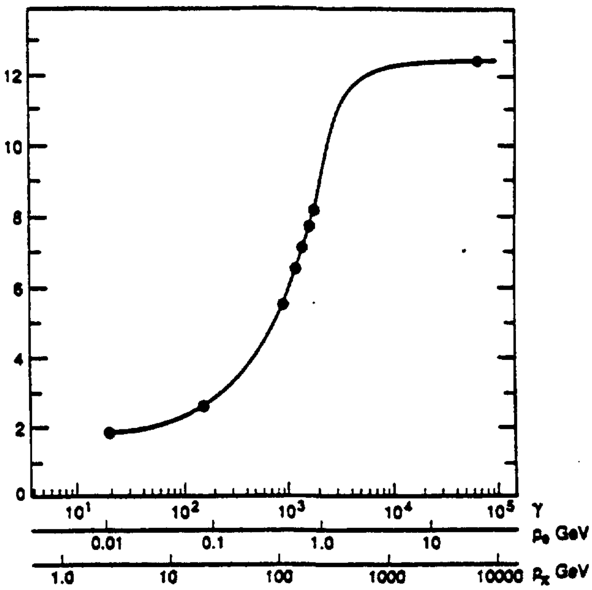

Fig. 24
Dependence of TR-yield (arbitrary units) on Lorentz-factor γ or particle type.

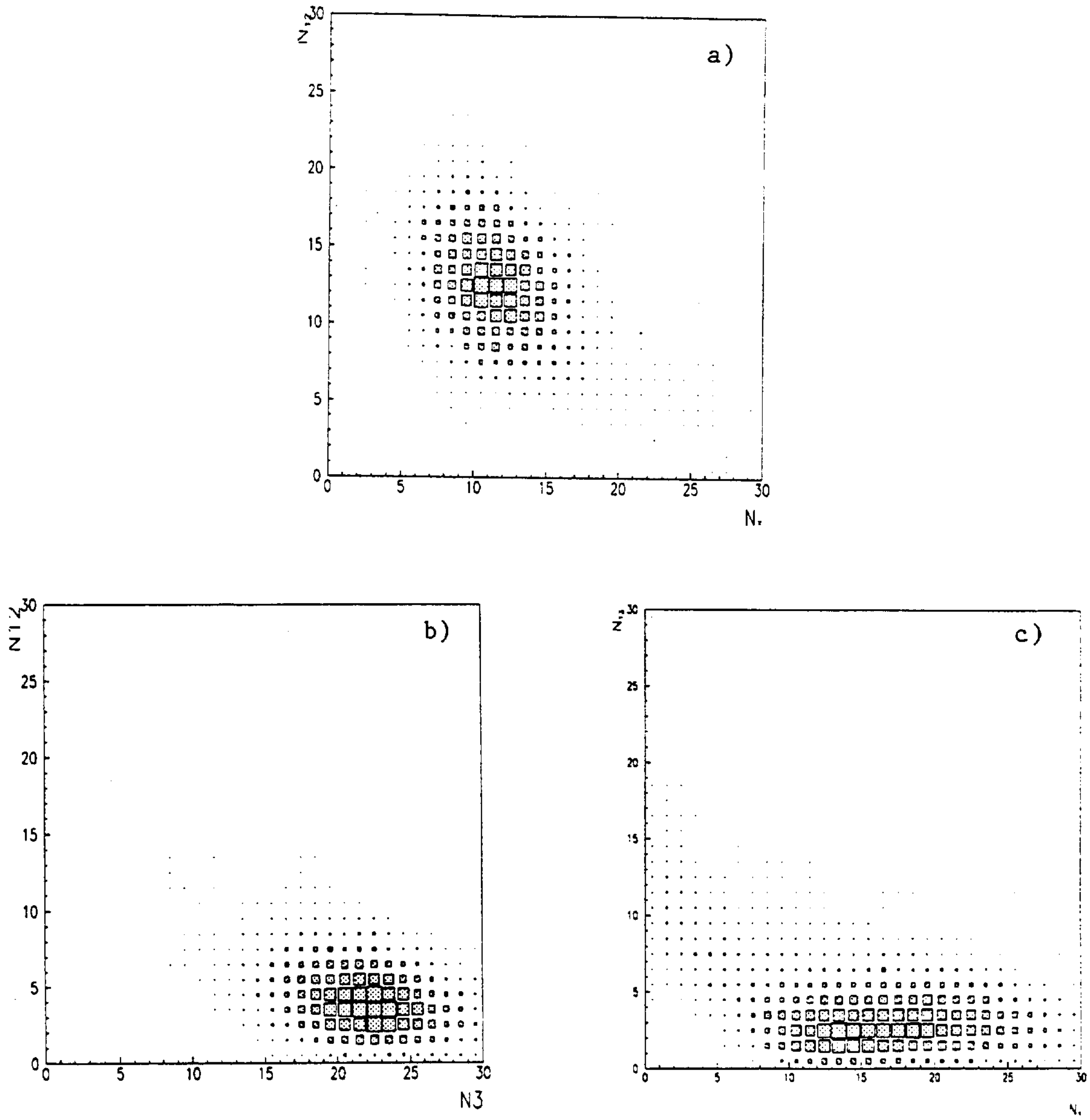

Fig. 25 Distribution of hits with energy between 0.2 and 1.5 keV (N_{12}) versus TR-hits (N_3) for 30 GeV electrons (a), closed photon conversions (b) and internal photon conversions (c).

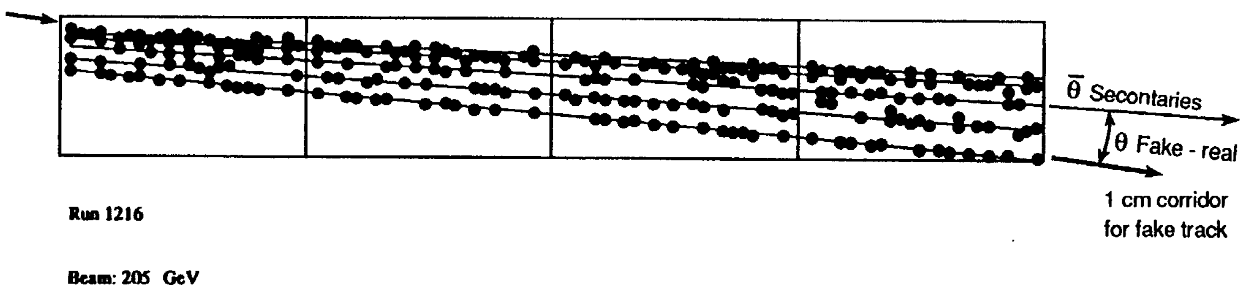

Fig. 26 Display of a target run event, with a typical 1 cm wide road for fake track searches.

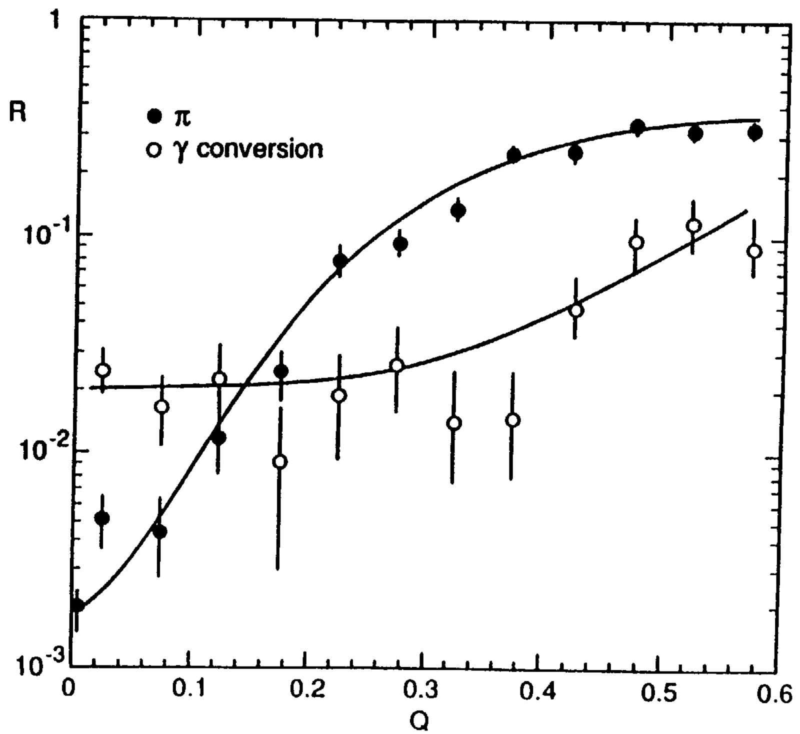

Fig. 27 Efficiency for detecting 20 GeV pions and external photon conversions as a function of straw occupancy.

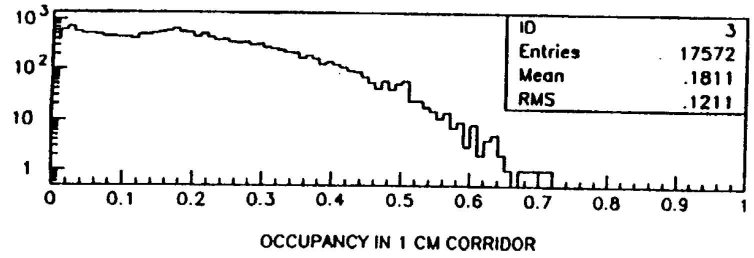

Fig. 28 Straw occupancy distribution in target run data.

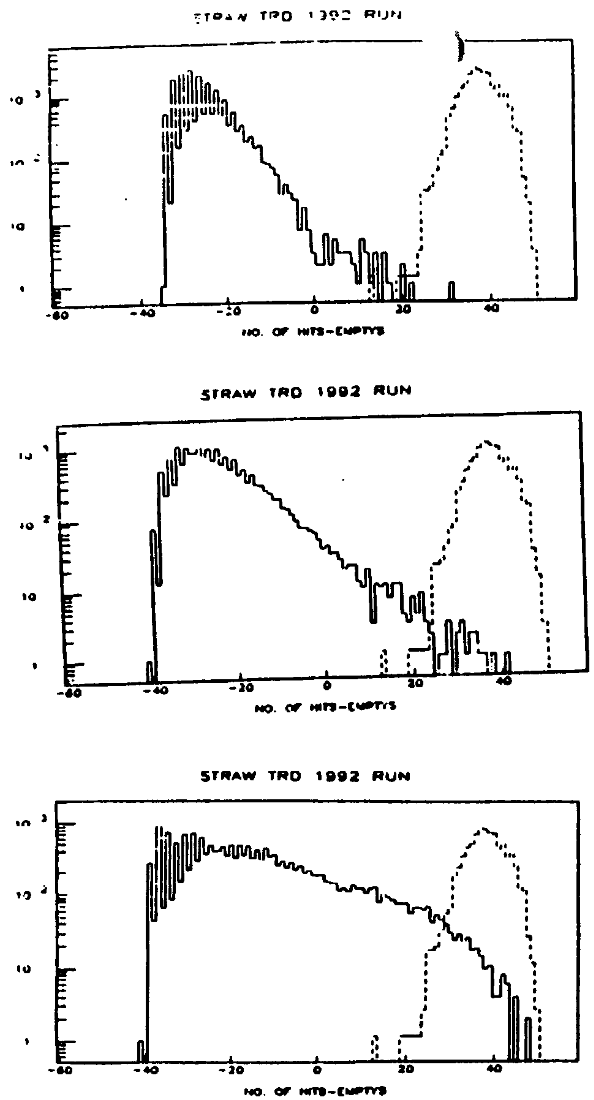

Fig. 29 Distribution of the difference between the number of hit straws and the number of empty straws for real tracks with angle θ_{REAL} and for fake tracks with angle θ_{FAKE}, for increasingy smaller values of the difference $\theta_{FAKE} - \theta_{REAL}$: 100 mrad (a), 50 mrad (b) and 10 mrad (c).

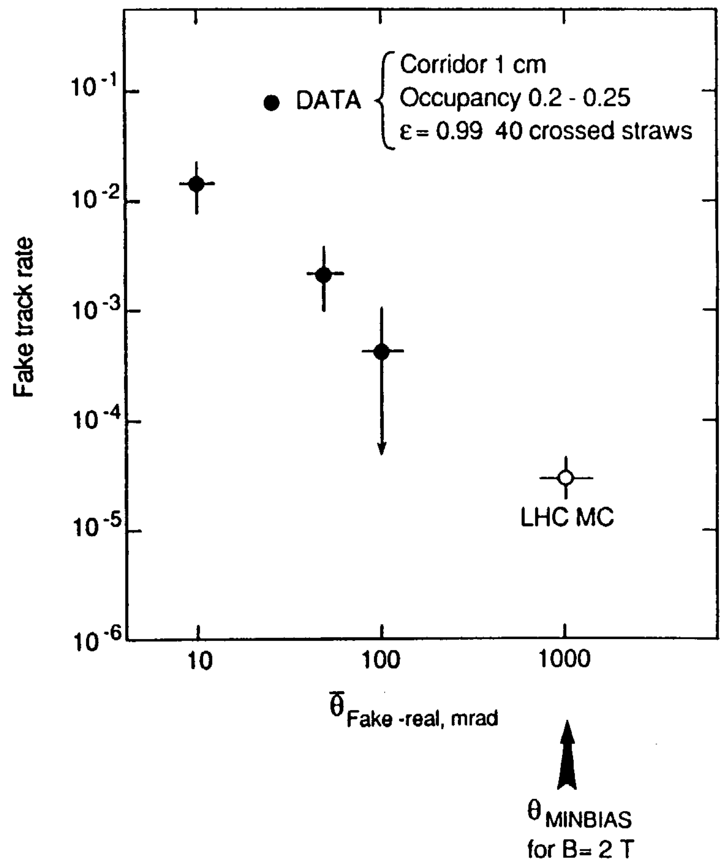

Fig. 30 Fake track rate for different degrees of hit correlations using target run data (see text) and MC for extrapolation to LHC.

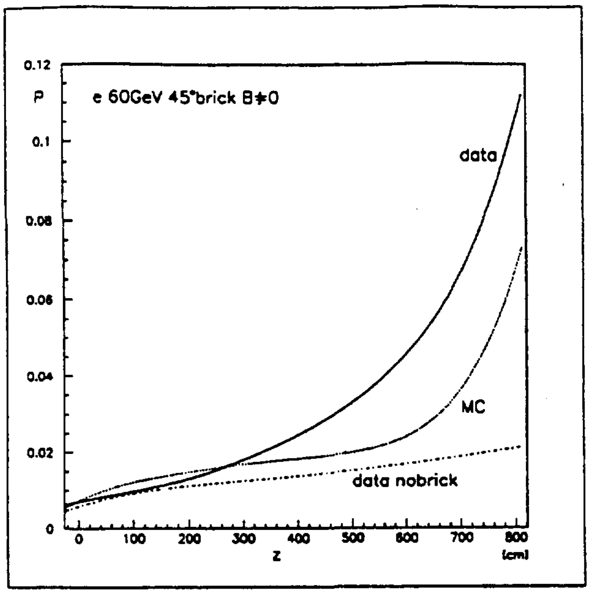

Fig. 31 Comparison of the straw hit probability between data (full line) and simulation (dotted line) outside the track road for 60 GeV electrons with a lead brick at an angle of 45º and with a magnetic field compared to data without backsplash (60 GeV electrons without brick and with magnetic field) indicated by the dashed line. The probability is shown as a function of z, the longitudinal position of the straws along the beam (large z corresponds to straws close to the lead brick).

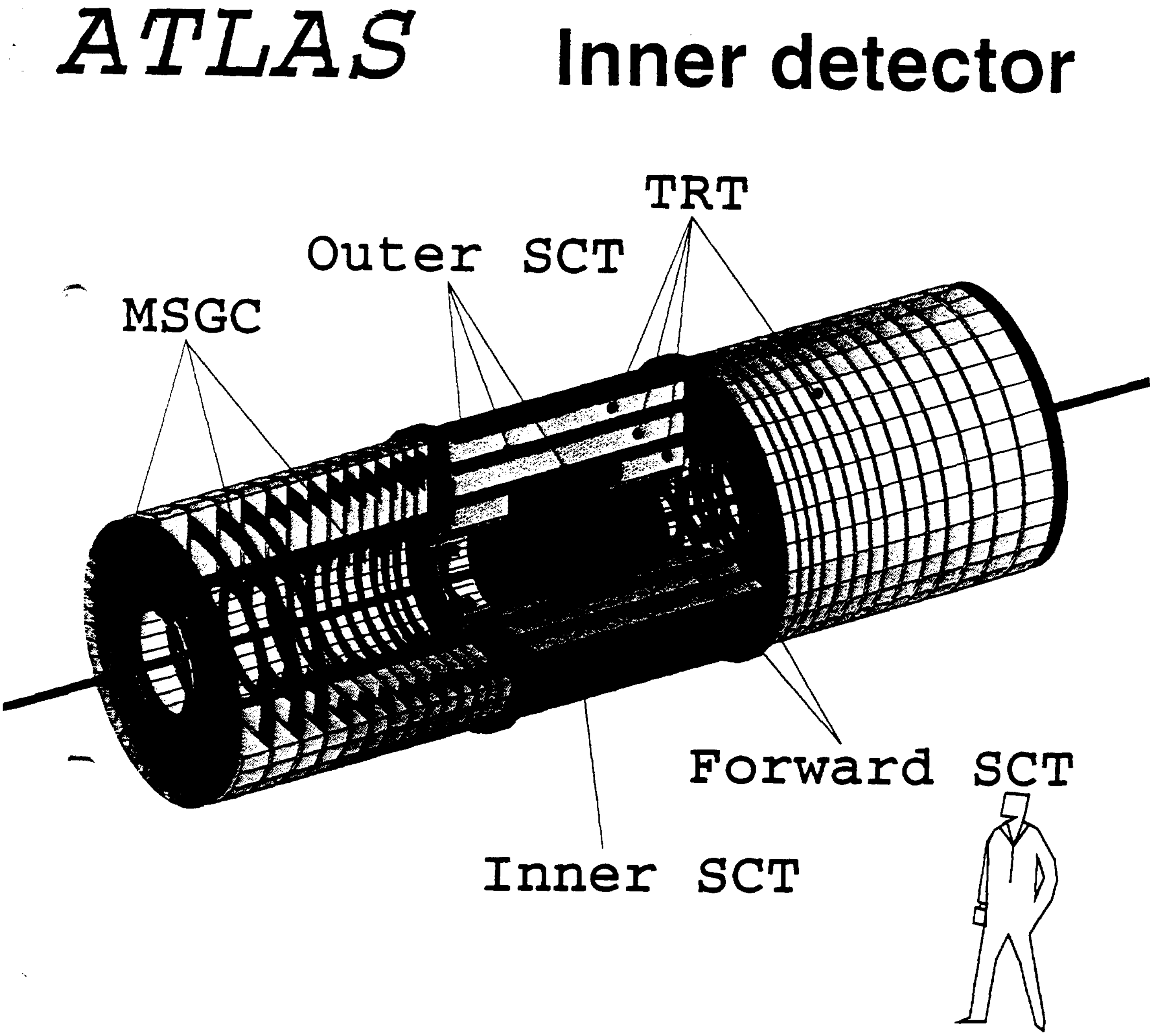

Fig. 32 Three-dimensional view of the TRT in the ATLAS inner detector.

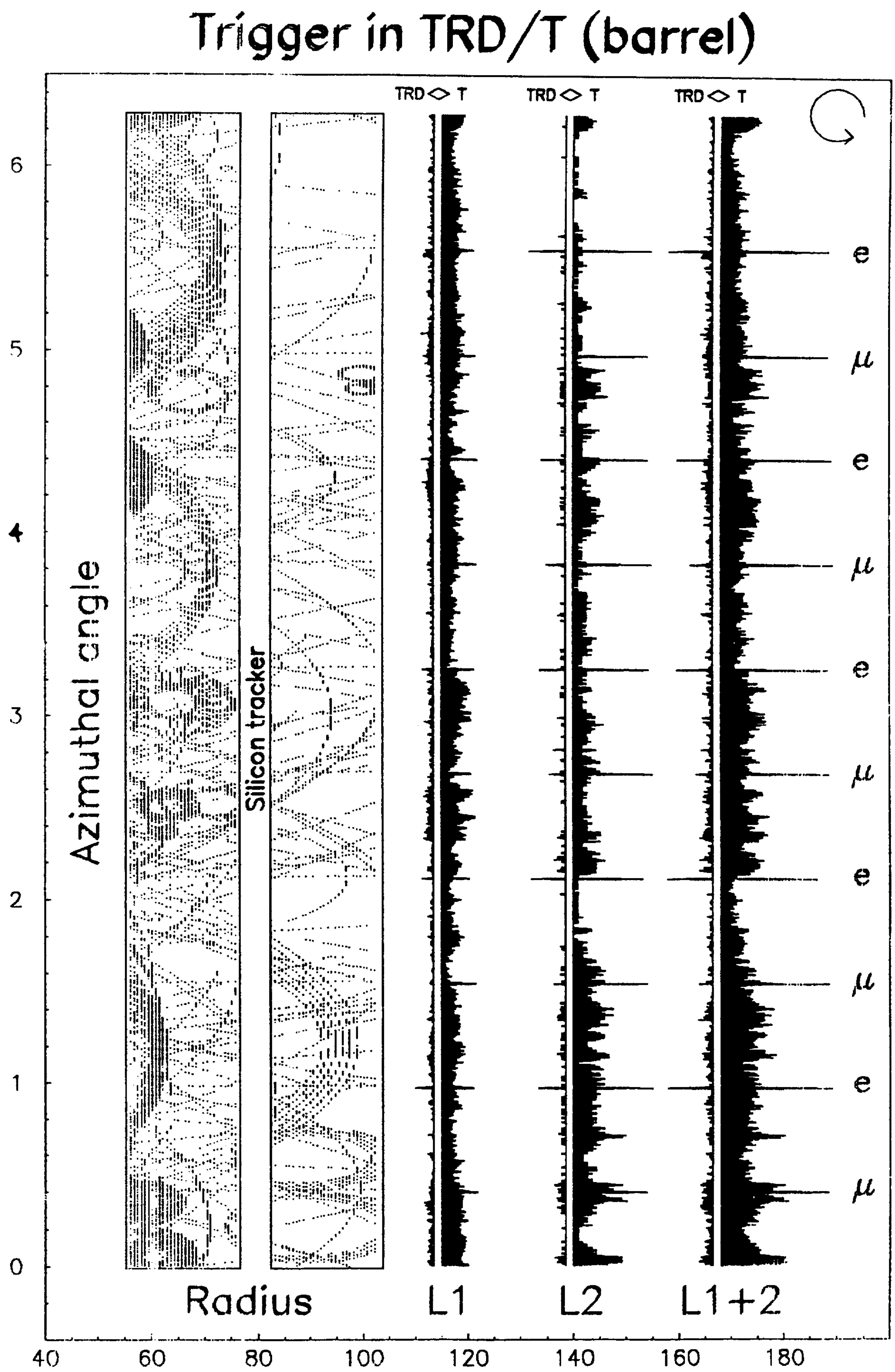

Fig. 33 Expected hit pattern in barrel TRT as a function of azimuth for a luminosity of 1.7 10^{34} $cm^{-2}s^{-1}$. Five electrons and five muons of 20 GeV are superimposed on top of the minimum bias pile-up. The histograms show the number of normal straw hits (right) and of TR-hits (left) as a function of azimuth for each of the barrel sectors (L1 and L2) and for the total (L1 + 2).

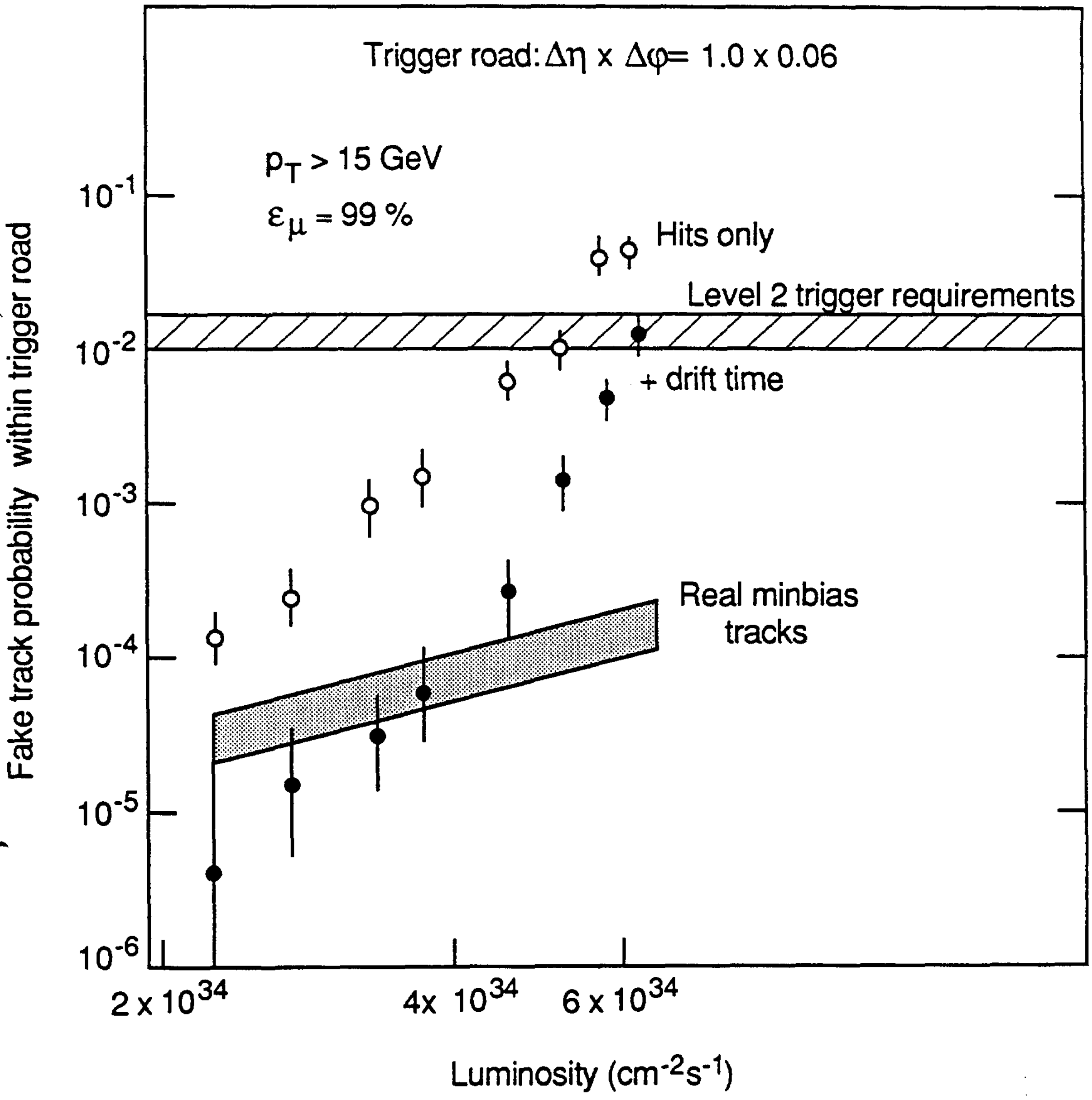

Fig. 34 Probability of finding fake tracks in the barrel TRT as a function of luminosity, using the raw hit information or using the full drift-time information.

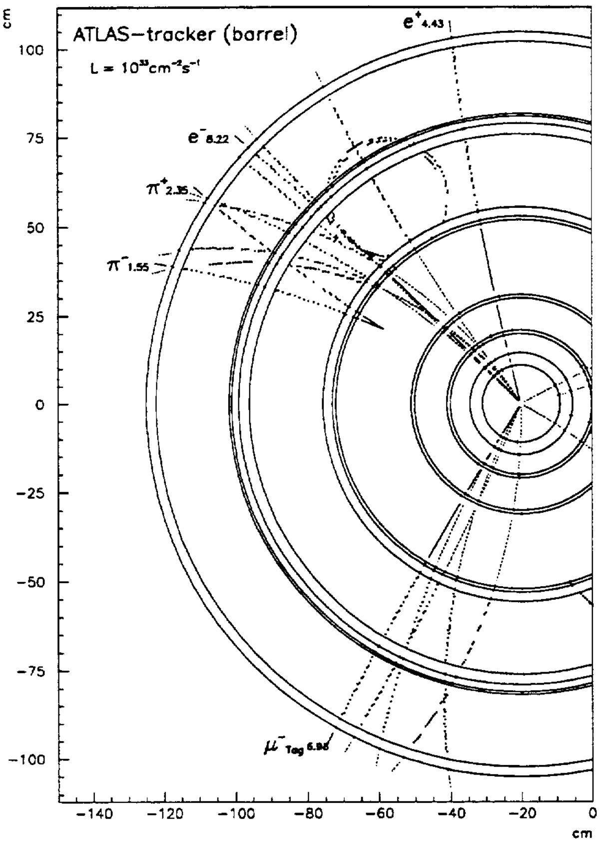

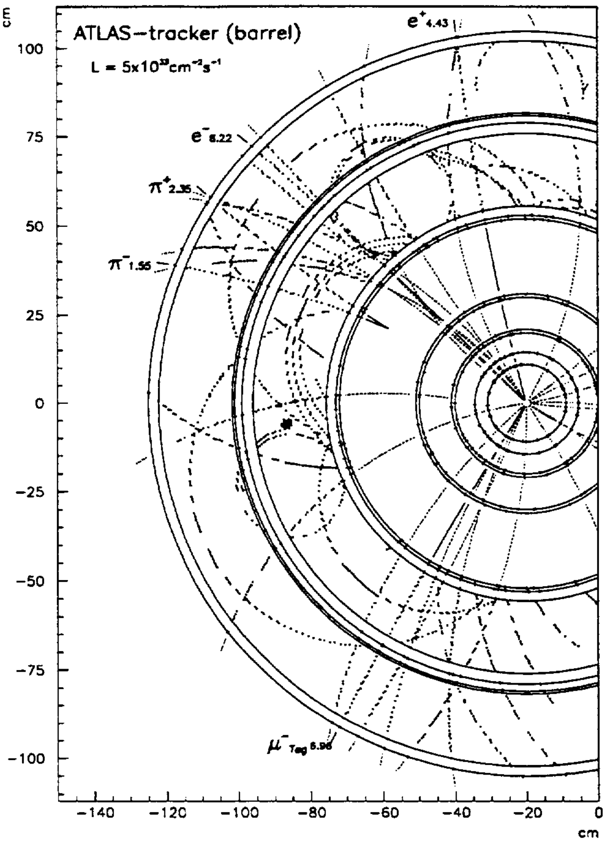

Figure 35: Display of one half of ATLAS barrel tracker in the transverse plane for a signal event from $B_d^0 \rightarrow J/\psi K_s^0$ decay at a luminosity L = 10^{33} $cm^{-2}s^{-1}$ (left), where two minimum bias events have been added on top of the signal event, and at a luminosity L = 5×10^{33} $cm^{-2}s^{-1}$ (right), where ten minimum bias events have been added on top of the signal event. The straw tracker hits are shown as large dots and the precision hits as dashes. The reconstructed tracks with $p_T > 0.5$ GeV and $0 < \eta < 0.8$ are shown as dotted lines between the detector planes and the interesting ones corresponding to the electrons from the J/ψ decay, the charged pions from the K_s^0 decay and the muon tag as full lines

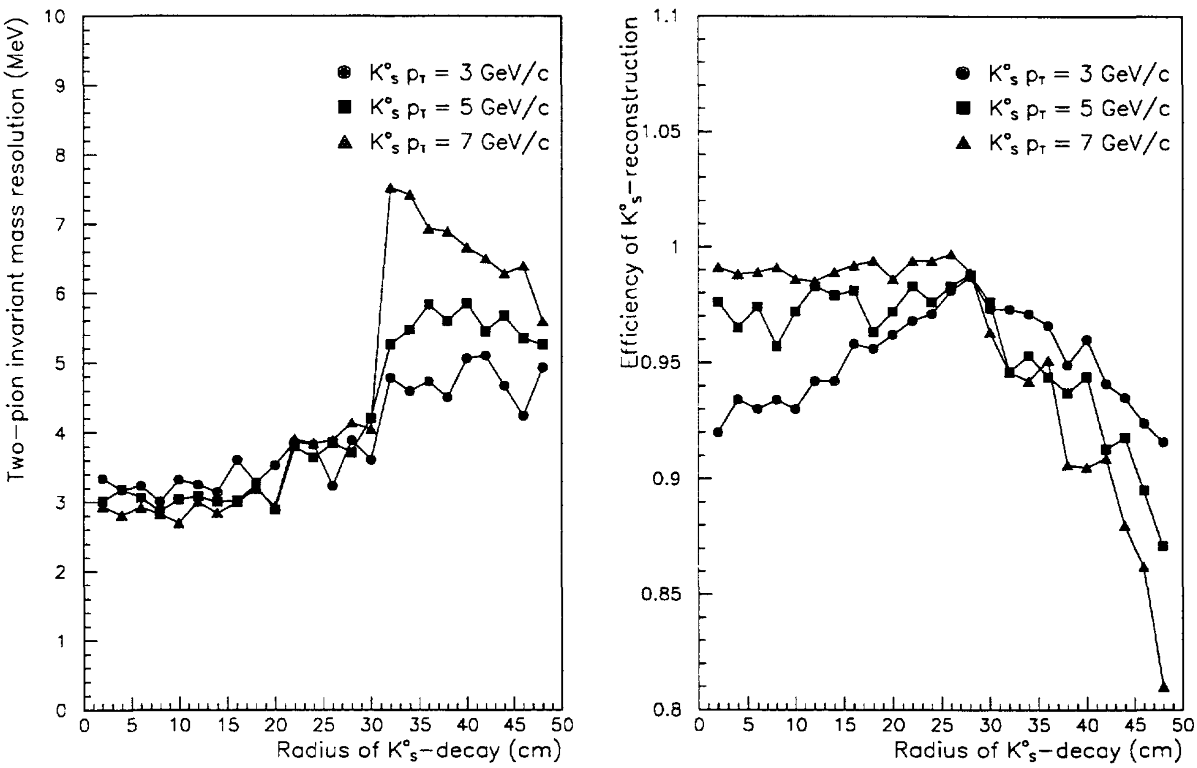

Figure 36: Mass resolution (left) and efficiency (right) for K_s^0 reconstruction as a function of K_s^0 decay radius R_d for three values of the K_s^0 p_T, typical of those expected for K_s^0 from $B_d^0 \rightarrow J/\psi K_s^0$ decays. The results are plotted after full simulation and reconstruction in the ATLAS barrrel tracker ($|\eta| < 0.8$). For $R_d = 30$ cm the mass resolution becomes worse by a factor ~ 2, due to the absence of any high-precision inner measurement for larger values of R_d. The drop in efficiency at small values of R_d for a K_s^0 p_T of 3 GeV is an artefact of the fiducial cuts used to define the barrel tracker acceptance. The drop in efficiency at large values of R_d and large values of the K_s^0 p_T is mainly due to the straw tracker two-track resolution

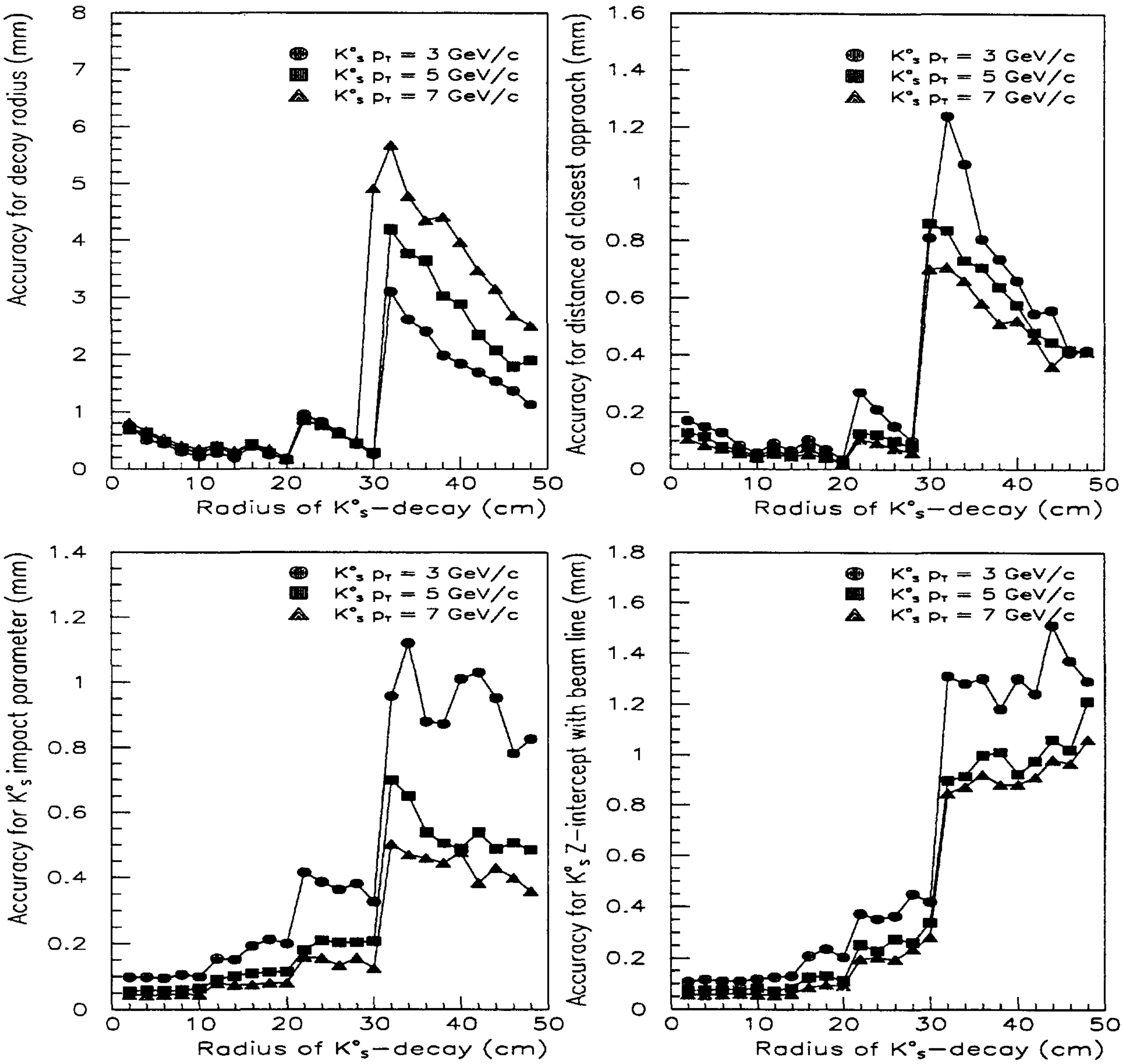

Figure 37: Accuracy of reconstruction of various parameters for K_s^0 decays as a function of the K_s^0 decay radius R_d and for three different values of the K_s^0 p_T, typical of those expected for K_s^0 from $B_d^0 \rightarrow J/\psi K_s^0$ decays. Shown are the accuracies for the reconstruction of the K_s^0 decay radius R_d (top left), of the distance of closest approach d_{min} between the two charged pion tracks (top right), of the K_s^0 impact parameter (bottom left) and of the longitudinal position of the intercept of the K_s^0 direction with the beam line (bottom left)

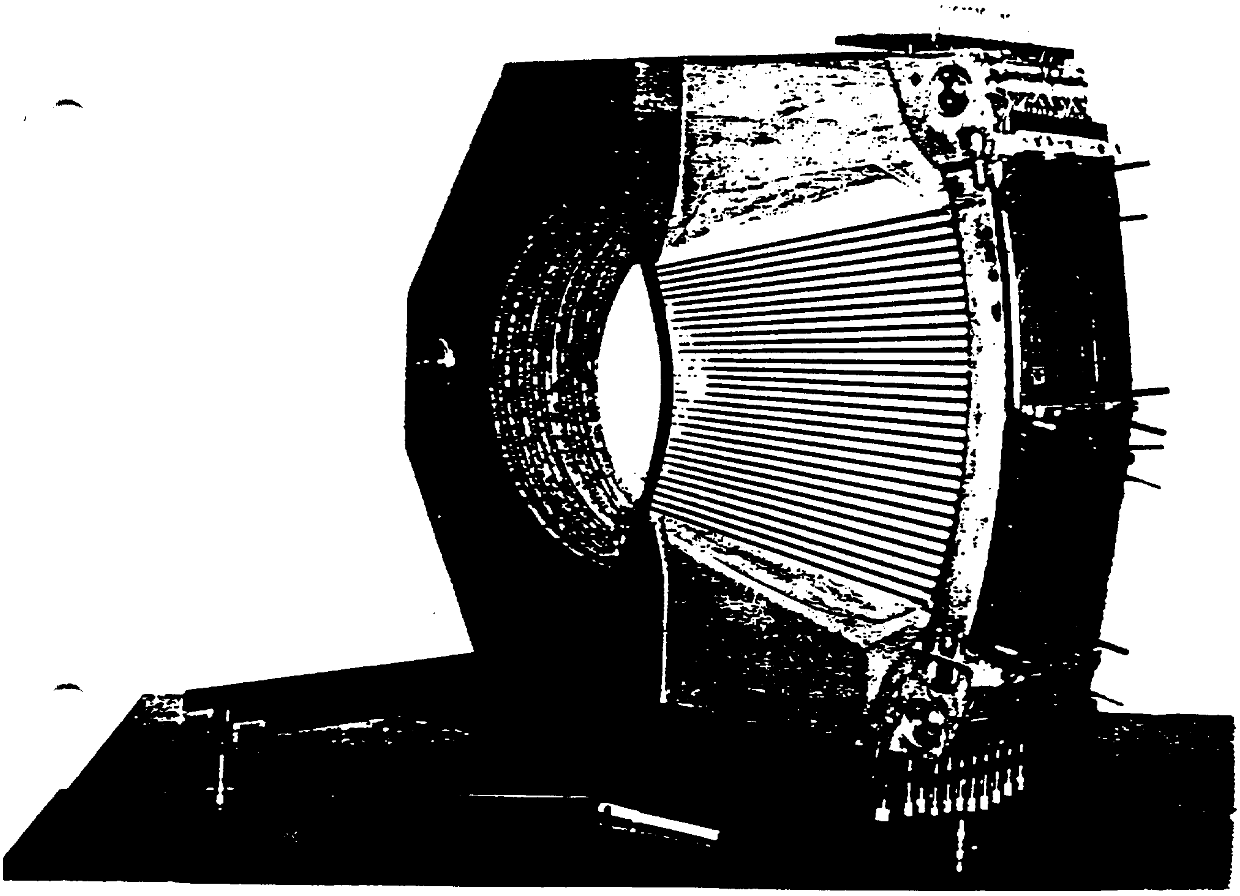

Fig. 38 Photograph of one block of sector prototype (512 straws).

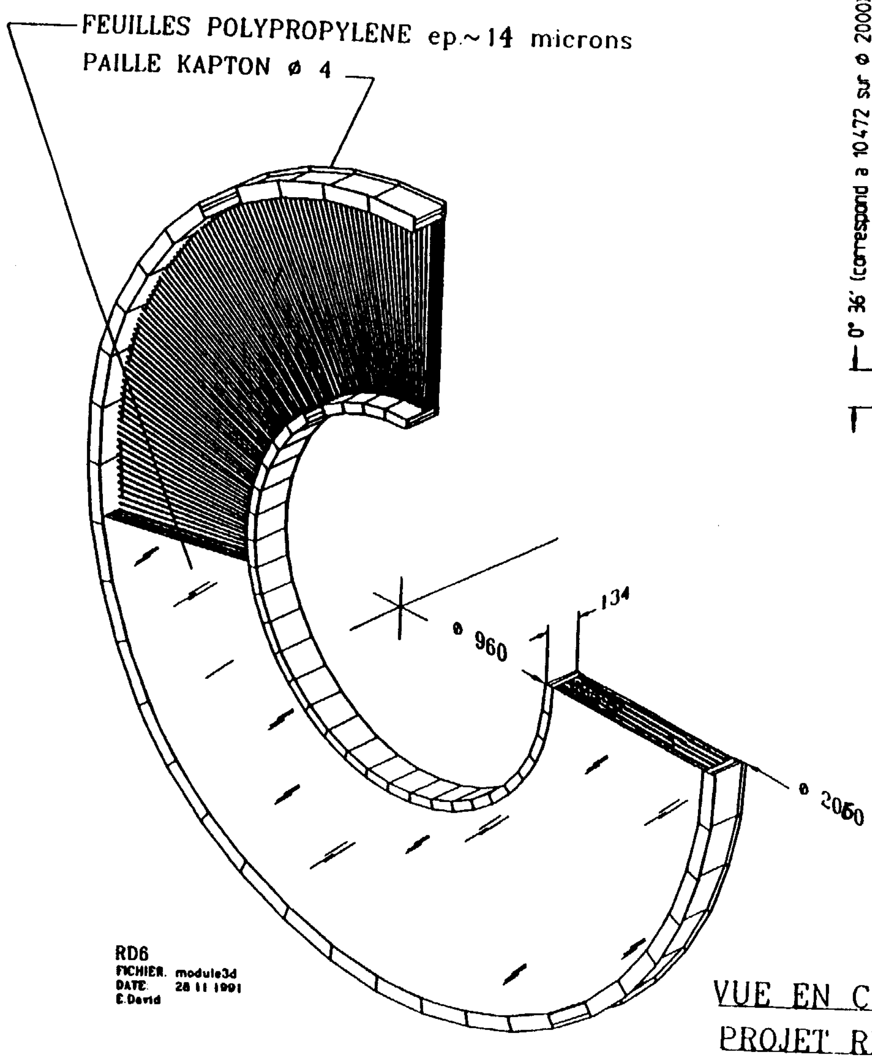

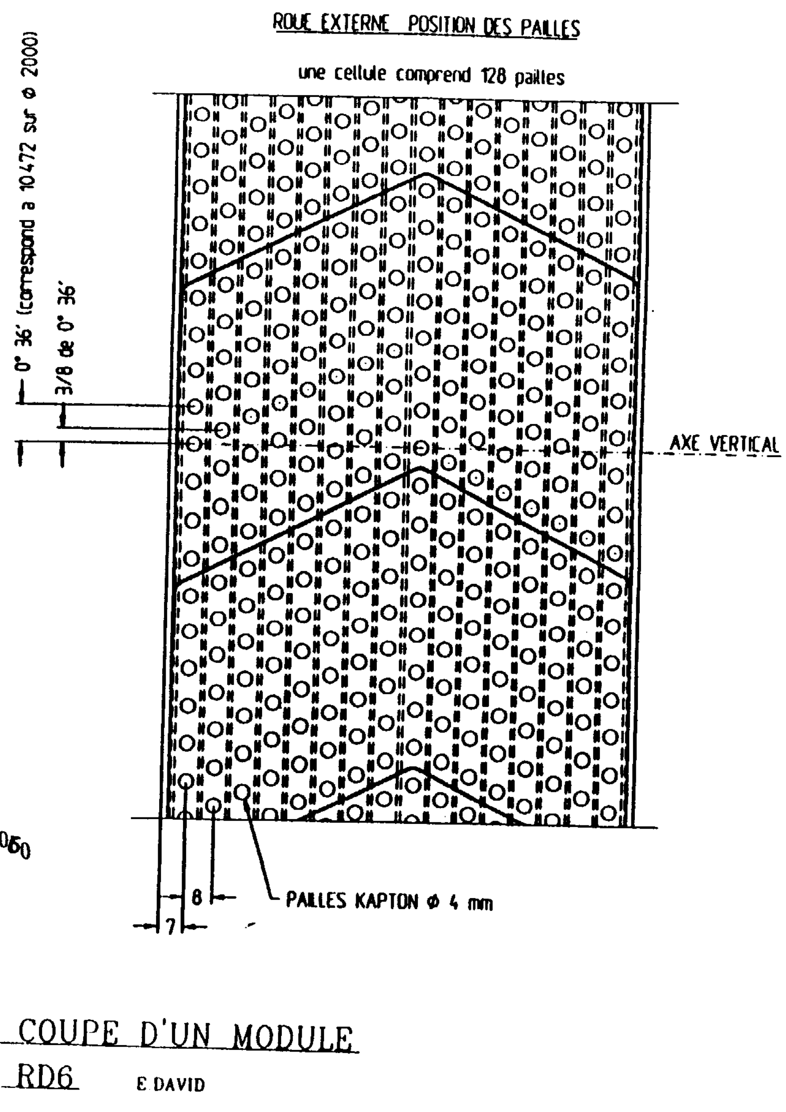

Fig. 39 One module ('wheel') of full scale ATLAS endcap TRT (left) and location of holes for straws on external ring (right).

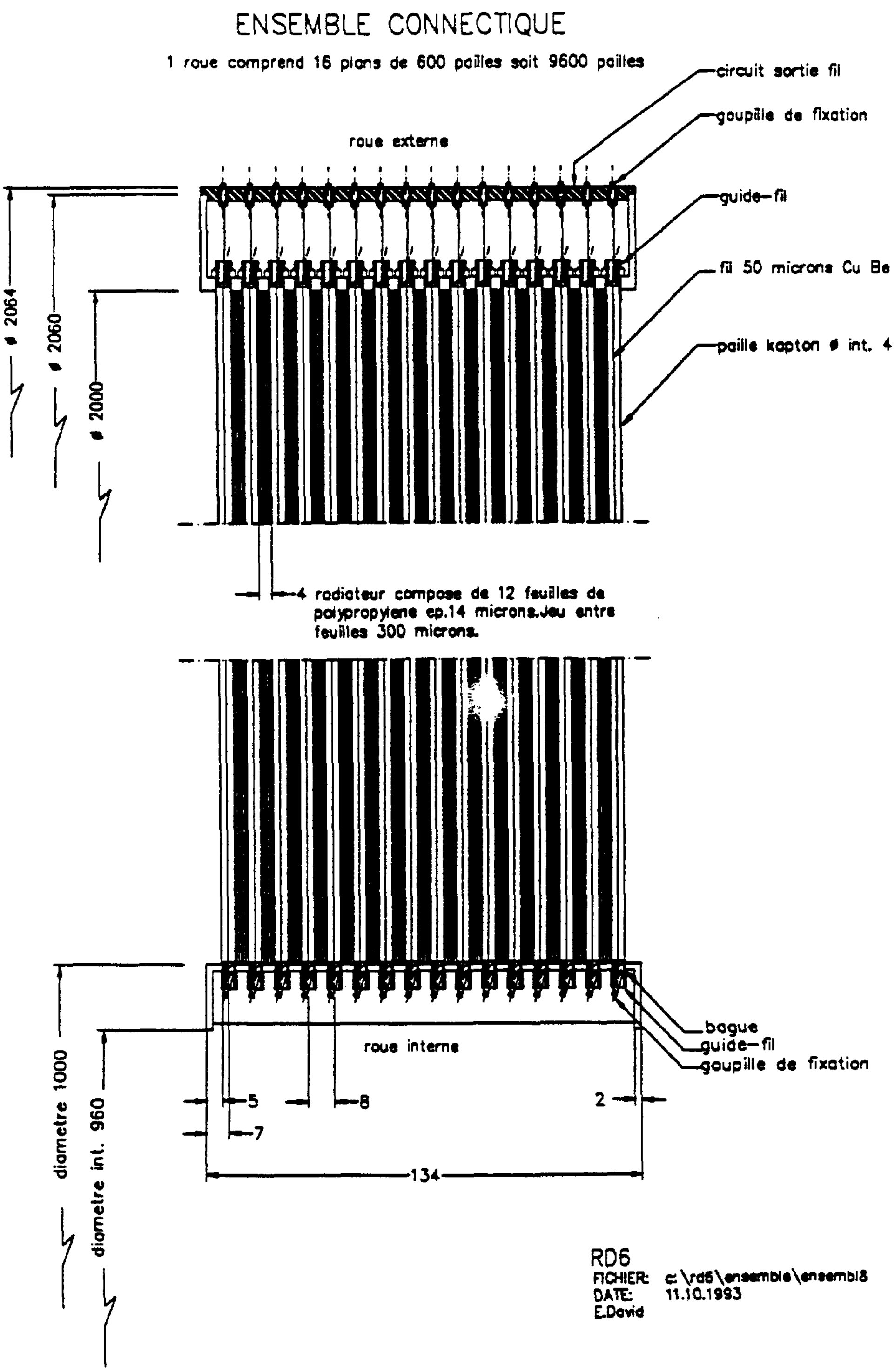

Fig. 40 Connection of straws and radiators to the inner and outer rings.

Dornier GmbH

Dornier
Deutsche Aerospace

CERN-Dornier
Inner/Outer Wheel for a TRD-Tracker

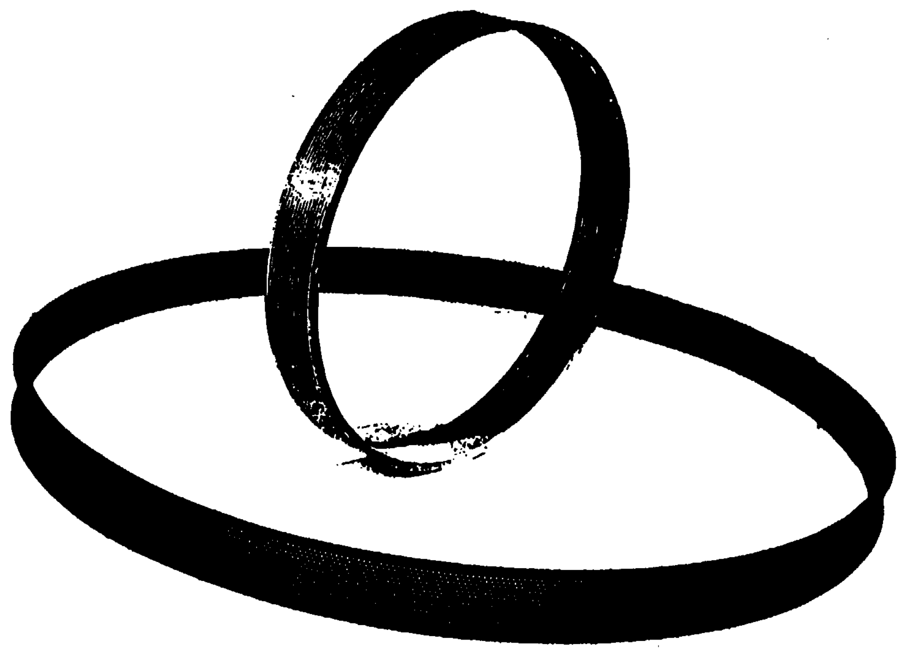

Fig. 41 Photograph of inner and outer rings as received from industry (Dornier).

Time measurer

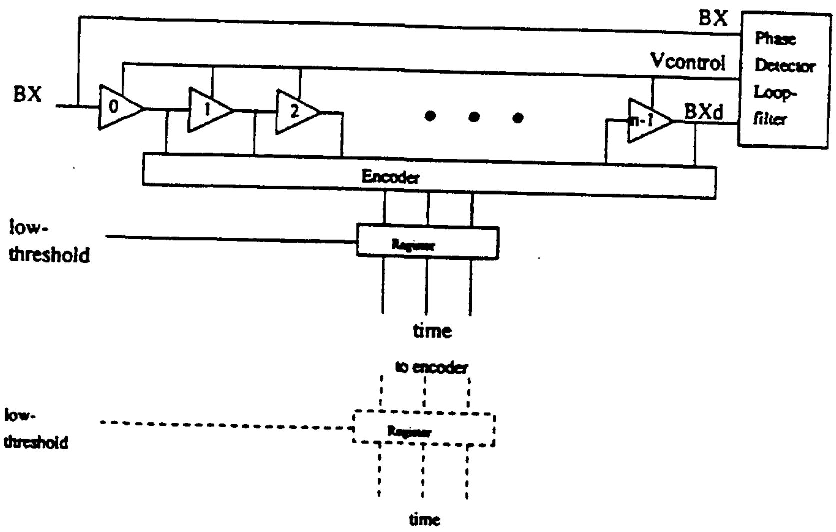

Fig. 42 Drift time measurement concept.

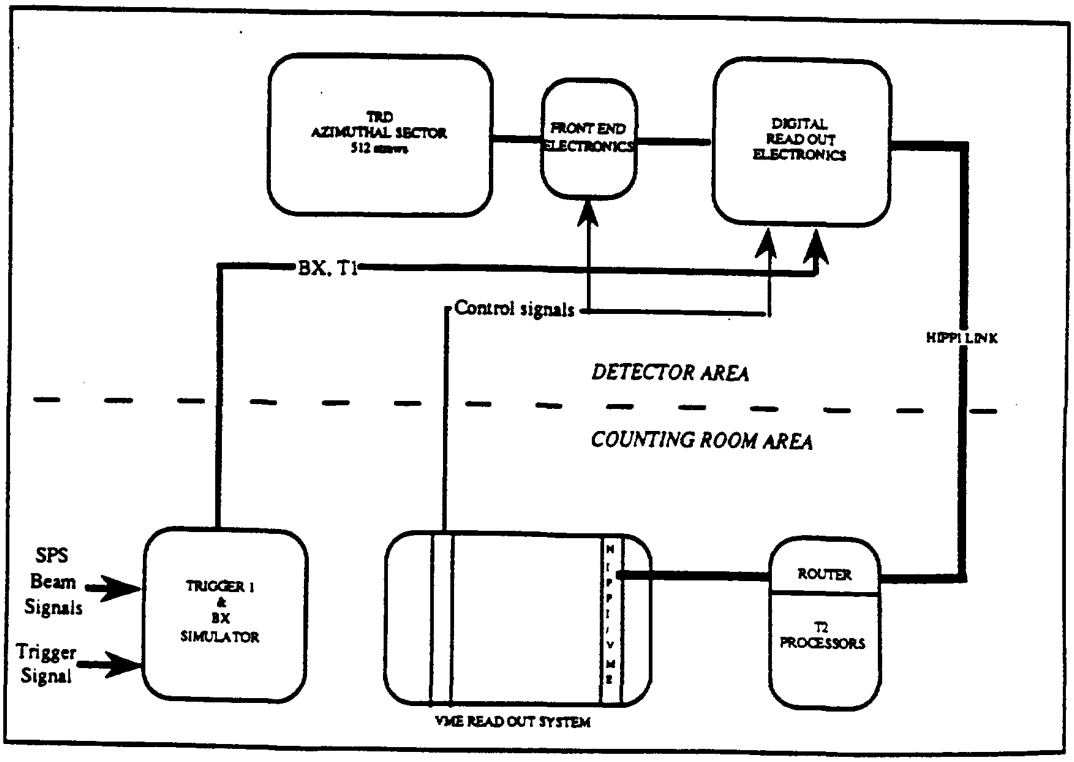

Fig. 43 Schematic layout of whole system.

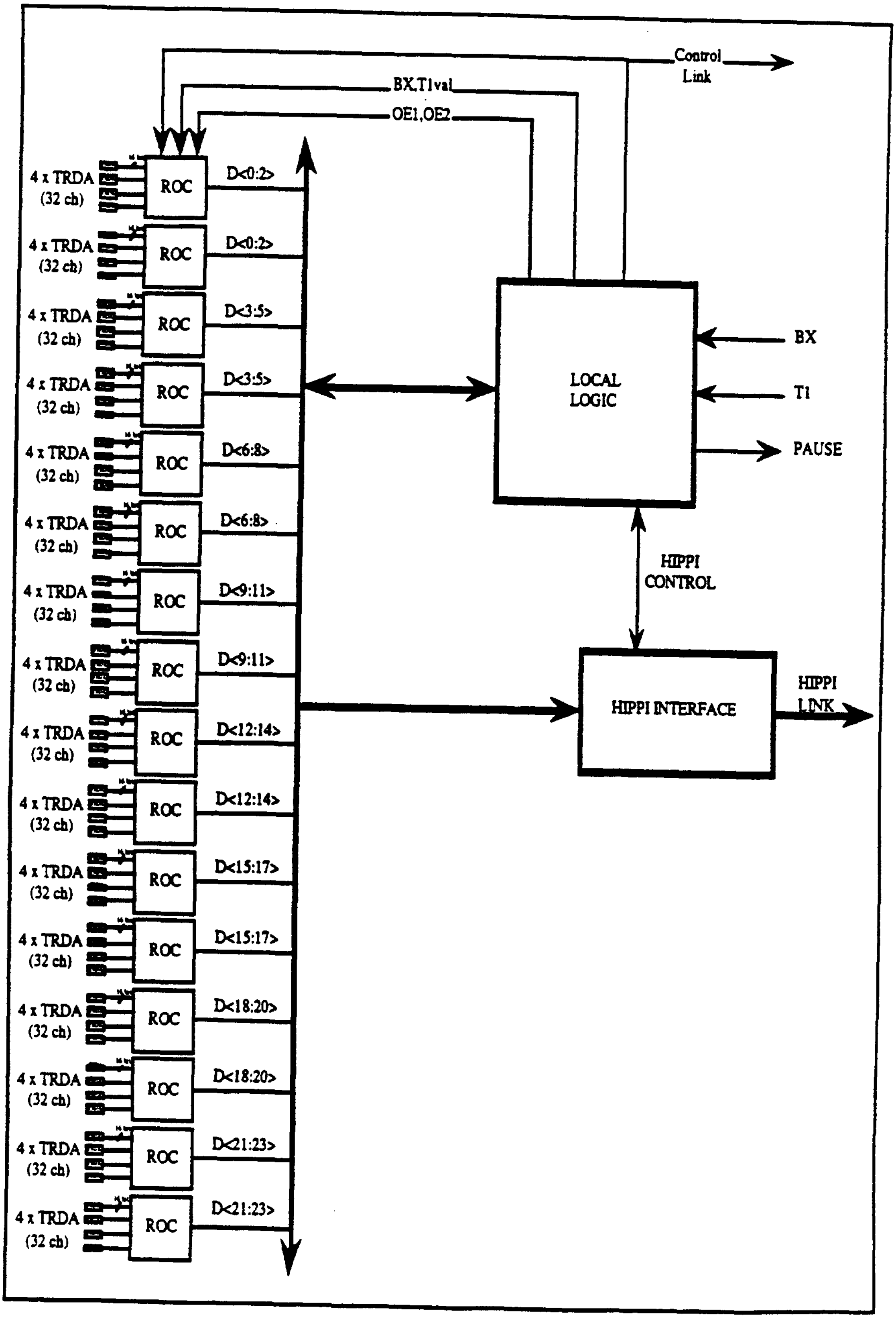

Fig. 44 Overview of the readout electronics.

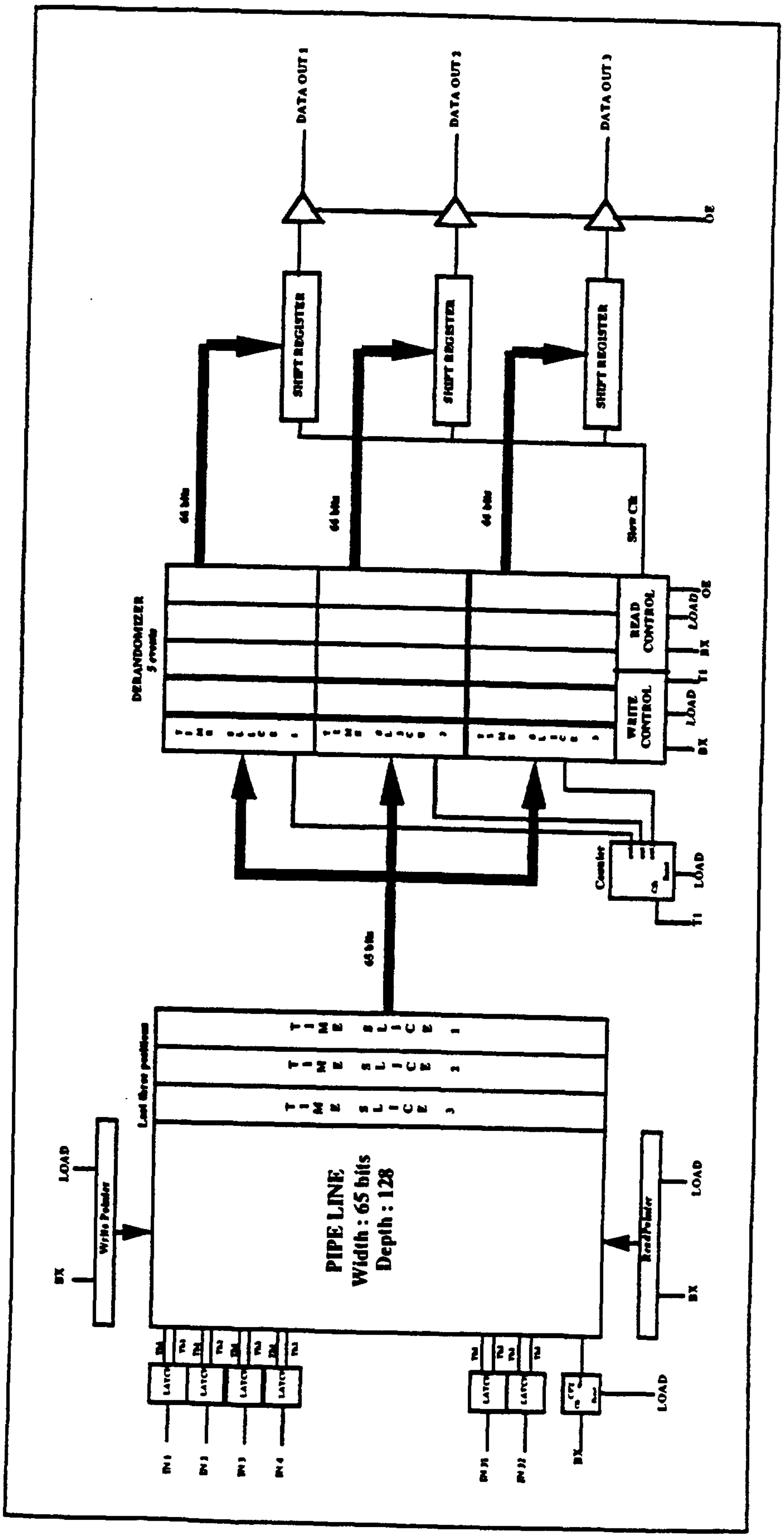

Fig. 45 Layout of the readout chip logic (ROC).

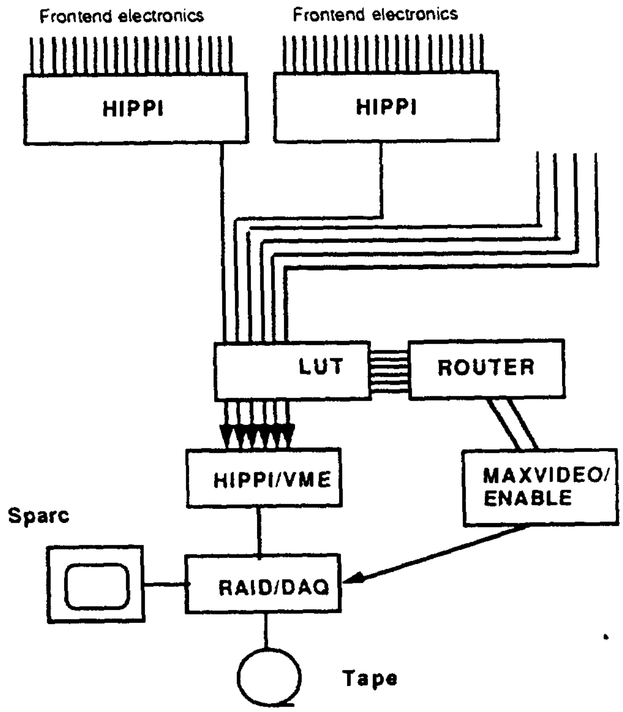

Fig. 46 Schematic layout of the level-2 trigger operation.